Published in final edited form as:
Bioorg Med Chem. 2014 August 1; 22(15): 4083–4098. doi:10.1016/j.bmc.2014.05.075.

Development of Radamide Analogs as Grp94 Inhibitors

Aaron Muth, **Vincent Crowley**, **Anuj Khandelwal**, **Sanket Mishra**, **Jinbo Zhao**, **Jessica Hall**, and **Brian S. J. Blagg***
Department of Medicinal Chemistry, The University of Kansas, 1251 Wescoe Hall Drive, Malott 4070, Lawrence, KS 66045-7563, United States

Abstract

Hsp90 isoform-selective inhibition is highly desired as it can potentially avoid the toxic side-effects of *pan*-inhibition. The current study developed selective inhibitors of one such isoform, Grp94, predicated on the chimeric and *pan*-Hsp90 inhibitor, radamide (RDA). Replacement of the quinone moiety of RDA with a phenyl ring (**2**) was found to be better suited for Grp94 inhibition as it can fully interact with a unique hydrophobic pocket present in Grp94. An extensive SAR for this scaffold showed that substitutions at the 2- and 4-positions (**8** and **27**, respectively) manifested excellent Grp94 affinity and selectivity. Introduction of heteroatoms into the ring also proved beneficial, with a 2-pyridine derivative (**38**) exhibiting the highest Grp94 affinity (K_d = 820 nM). Subsequent cell-based assays showed that these Grp94 inhibitors inhibit migration of the metastatic breast cancer cell line, MDA-MB-231, as well as exhibit an anti-proliferative affect against the multiple myeloma cell line, RPMI 8226.

Introduction

Heat shock protein 90 (Hsp90) is a molecular chaperone that plays an important role in cellular activity by maintaining the conformational maturation of approximately 200 client proteins. In normal cells, Hsp90 is associated with proteins responsible for trafficking, cell signaling, protein folding, as well as the maintenance and degradation of client proteins.[1,2] Hsp90 functions are modulated through three domains; the N- and C-termini and the middle domain. The N-terminus contains an ATP-binding site which upon binding ATP closes to induce ATP hydrolysis and provides the chaperone machinery the energy required for protein folding. The middle domain binds the γ-phosphate of ATP and is responsible for interactions with client proteins. The C-terminus controls Hsp90 homodimerization and also contains a nucleotide-binding site that allosterically regulates the N-terminal domain.[3–9] In cancer cells, Hsp90 is overexpressed and involved in numerous pathways required for the rapid growth and proliferation of cancer cells. As a consequence of its essential role in so many processes, Hsp90 is a highly sought after therapeutic target, as disruption can simultaneously affect multiple pathways required for cancer cell growth.[10–12, 42–50]

*Corresponding author; Phone: (785) 864-2288. Fax: (785) 864-5326. bblagg@ku.edu.

Supplementary Data
Supplementary data associated with this article can be found in the online version at

Hsp90 N-terminal inhibition has been shown to be an effective therapeutic strategy as 17 inhibitors of the ATP-binding site have advanced to clinical trials for the treatment of various cancers. Despite the number of N-terminal inhibitors in clinical trials, detrimental activities that include cardiovascular, ocular, and/or hepatotoxicities, amongst others have been observed for many of these investigational new drugs.[13–15] Unfortunately, the N-terminal ATP-binding site is >85% identical across all four Hsp90 isoforms, which includes cytosolic Hsp90α and β, the endoplasmic reticulum-localized isoform, Grp94, and the mitochondrial chaperone, Trap1.[16] Since *pan*-inhibition of all Hsp90 isoforms can result in the degradation of more than 200 Hsp90-dependent client proteins, it is likely that toxic side effects cannot be overcome by traditional approaches that focus upon *pan*-Hsp90 inhibition. Recently, it was shown that Hsp90α is the isoform responsible for maturation of the hERG channel, and is therefore more likely responsible for the clinically observed cardiotoxicity.[17] Consequently, new approaches toward Hsp90 inhibition are needed in an effort to refine the number of Hsp90-dependent proteins as well as to escape the deleterious consequences of *pan*-Hsp90 inhibition. The development of isoform-selective Hsp90 inhibitors represents an attractive strategy for the discovery of such attributes.

Compared to cytoplasmic Hsp90 α and β, the biological role manifested by glucose regulated protein-94 kDa (Grp94) is far less explored.[16] Preliminary studies on Grp94 indicate that many of its client proteins are involved in intercellular communication and adhesion (i.e. Toll-like receptors, myocilin, integrins, immunoglobulins).[18] These properties suggest that Grp94 inhibition may be useful for the treatment of specific disease states. For example, since Grp94 plays an integral role in the trafficking of integrins to the cell membrane, it represents a potential target for the development of anti-metastatic agents.[19] This is further illustrated by recent work showing that Grp94 inhibition (via siRNA knockdown) led to inhibition of cell proliferation, migration and metastasis in two aggressive breast cancer cell lines (MDA-MB-231 cells and reactive oxygen species resistant (ROS) MCF-7 cells).[20] Grp94 has also been ascribed a role in glaucoma due to its involvement in mutant myocilin clearance.[21] In addition, Grp94 was found to be overexpressed in multiple myeloma as a consequence of endoplasmic reticulum stress,[22–24] in fact, Grp94 inhibition was shown to decrease the proliferation rate of multiple myeloma cells.[25]

Despite the highly homologous nature of Hsp90 isoforms, Grp94 possesses a five-amino acid insertion (QEDGQ) between residues 182 and 186, which translates into a small pocket that can be accessed by Grp94 inhibitors.[29] This insertion does not exist in other Hsp90 isoforms, and therefore creates a unique hydrophobic environment within the ATP-binding domain that can lead to selective inhibition.[26–29] In 2009, a novel mode of binding was identified for the radicicol/geldanamycin chimeric inhibitor, radamide (RDA)[30,31,37–40] bound to Grp94 (Figure 1). Co-crystal structures of RDA bound to both Hsp90 and Grp94 (Figure 1)[30] indicated two key elements were needed to target the hydrophobic binding pocket and to selectively bind Grp94. The first proposed modification included replacement of the quinone ring with a phenyl substituent that interacts favorably with the hydrophobic pocket exclusive to Grp94. The second requirement for binding to Grp94 was projection of the phenyl group into this hydrophobic environment. Such observations led to the

development of BnIm, which demonstrated good Grp94 inhibitory activity in a number of assays.[26] However, little effort towards the development of RDA as a Grp94 inhibitor has been pursued, until now. Therefore, the goal of this project was to further evaluate RDA as a Grp94 inhibitor and to establish structure-activity relationships for this class of inhibitors.

Results and Discussion

Optimization of the RDA scaffold required several modifications to access the unique hydrophobic pocket within Grp94. The first investigation needed to determine the optimal linker length between the amide and the aromatic ring that projects into the hydrophobic pocket (compounds **2–5**) as suggested by Figure 1. This is necessary to determine how deep these molecules can project into the pocket and to provide a scaffold upon which substituents can be readily incorporated for elucidation of structure-activity relationships. Substitutions around the aryl ring would then probe for beneficial interactions with the peptide binding pocket as outlined in Scheme 1. These observations led to the design and synthesis of compounds that would provide an initial set of data to direct subsequent optimization efforts. Since RDA bound to Grp94 (Scheme 1) indicated an extended π-stacking environment with Phe199 and Tyr200, naphthyl, indole, and indoline scaffolds were also pursued to take advantage of potential interactions. These aryl systems could then be modified to contain additional substitutions about the ring for further access into the **A** and **B** pockets. Due to π-π interactions with Phe199 and Tyr200, probing the electronic nature of the aryl ring via the addition of heteroatoms that could enhance interactions was also investigated and led to the identification of additional compounds. Lastly, since the *cis*-amide conformation was found important for binding Grp94 (Figure 1), tertiary amides were prepared to promote the *cis*-conformation.

Projection of the phenyl ring into the hydrophobic binding region (Scheme 1) required optimization of the linker length between the amide and phenyl groups, leading to the synthesis of **2–5** (Figure 2). Molecular modeling studies indicated that phenyl amide **2** would provide the ideal linker for binding Grp94. In an effort to validate this model and to support this hypothesis, linkers between the amide and the phenyl ring were synthesized and analyzed for inhibitory activity. In the event, TBS-protected acid **1**, was coupled with the corresponding aniline, benzylamine, phenethylamine, or phenyl hydrazine, utilizing 1-ethyl-3-(3-dimethylaminopropyl)carbodiimide (EDCI) and pyridine in dichloromethane, to generate the corresponding amides . These compounds were subsequently treated with tetrabutylammonium fluoride (TBAF) to unmask the phenols, **2–5**, in good yields. These compounds were evaluated for their ability to bind Grp94 via a competitive binding fluorescence polarization assay (Figure 2).[32,33] As suggested by computational studies, phenyl amide **2**, was found to contain the optimal linker as compared to benzyl amide, phenethyl amide, and hydrazine amide (**3, 4**, and **5**, respectively). As described earlier, RDA analogs appear to manifest π-π interactions with Phe199 and Tyr200, therefore, compound **6**, containing a cyclohexyl ring in lieu of the phenyl ring, was synthesized and evaluated. As expected, this compound demonstrated a decrease in binding affinity (compound **2** Grp94 K_d, 20.5 μM, compound **6** Grp94 K_d, 35.2 μM), which was in accord with our predictive model that supported π-π stacking interactions between Grp94 and compound **2**. These

studies validated compound **2** as our starting point for further development and allowed further interrogation of this scaffold.

Functionalization of phenyl amide **2** at the 2-, 3-, and 4-positions was pursued to explore the space surrounding the phenyl ring and to identify key interactions by the inclusion of electron donating and withdrawing groups. As seen in Scheme 1, there are two main pockets (**A** and **B**) within the hydrophobic binding region. Molecular modeling indicated that the 2-position of the phenyl ring is directed towards pocket **A**, whereas the 3- and 4-positions point at **B**. Substitutions at these positions could also provide information about the potential for π-stacking and hydrogen bonding interactions.

Functionalization of **2** at the 2-position on the phenyl ring was pursued with the goal of projecting substituents into pocket **A** and/or altering the electronic nature for additional π-π interactions. EDCI-mediated coupling with the corresponding anilines, **7a–15a**, followed by silyl-deprotection, generated amides **7–15** in good yields. Evaluation of **7–15** by the fluorescence polarization assay demonstrated enhanced binding affinities for these compounds (≤20% tracer bound) as compared to the unsubstituted lead compound. These substitutions illustrated that both electronic and steric effects influence the ability of these amides to bind Grp94, and the 2-chloro exhibited the highest affinity (**8**, 0.1% tracer bound). A trend is observed in Figure 3 which suggests that substituents larger than chlorine (for example, 2-bromo and 2-trifluoromethyl, compounds **9** and **11**, respectively) exhibit a size-dependent decrease in binding affinity. The 2-fluoro derivative, **7**, also exhibited a decrease in binding affinity, which may result from its inability to fill this hydrophobic environment. However, this could also be a consequence of the electronic effects manifested by fluorine, which prevents the amide bond from adopting the *cis*-conformation.[34] Electron donating groups, hydrogen bond acceptors and hydrogen bond donors all exhibit a decreased affinity for binding Grp94. Ultimately, it was discovered that a chlorine atom at the 2-position (compound **8**) proved optimal for binding to pocket **A**.

Additional structure-activity relationships were pursued by the incorporation of substitutions at the 3-position of the phenyl ring. As shown in Scheme 1, the 3-position of the phenyl ring provides access to pocket **B** and therefore, substitutions were incorporated to elucidate the size of this pocket, the electronic nature that can enhance π-π stacking interactions, and potentially, hydrogen bonding interactions with Gly196. This led to the synthesis of 3-substituted amides by an EDCI-mediated coupling of acid **1** with the corresponding anilines, **16a–24a**, followed by silyl-deprotection to give the desired amides, **16–24**, in good overall yields. As seen in Figure 4, these substitutions followed a similar trend for Grp94 binding as observed for the 2-position, as chlorine at the 3-position (**17**) displayed the highest binding affinity for Grp94. In comparison, larger (compounds **18–20**) and smaller (compound **16**) substituents resulted in diminished binding. In contrast to the 2-position, incorporation of a hydroxyl or amino group at the 3-position (compounds **21** and **22**, respectively) led to increased affinity for Grp94 (potentially through a gained hydrogen bonding interaction with Gly196). Both amino and *N*-acetamides manifested decreased binding affinity as compared to the phenol, as they are known to form weaker hydrogen bonds. Ultimately, the 3-chloro derivative proved to bind Grp94 more efficiently than the 3-phenol, indicating a preference for hydrophobic over hydrogen bonding interactions at this location.

The 4-position of the phenyl ring was also explored by the introduction of electron donating and withdrawing groups. As indicated in Scheme 1, the 4-position appears optimal for directing substituents into pocket **B**, however, a potential hydrogen bonding interaction with Gly196 could also be rationalized. Similar to 3-substitutions, the 4-position was investigated for steric constraints in pocket **B**, as well as elucidation of the electronic nature for π-π interactions with Phe199 and Tyr200. Compounds **25–37** were synthesized via EDCI-mediated coupling of TBS-acid **1** with the corresponding anilines, **25a–37a**, followed by silyl-deprotection to provide amides **25–37** in good overall yields. When evaluated for their ability to bind Grp94, the 4-position followed a very clear SAR trend with particular sensitivity to sterics (as shown in Figure 5). In contrast to the 2- and 3-positions, the 4-position appears to accommodate larger functionalities, as illustrated by the inclusion of bromine at the 4-position (compound **27**), which displayed excellent affinity for Grp94. The enhanced affinity for **27** was anticipated as the 4-bromine can project well into the hydrophobic pocket of area **B** (Scheme 1). A decrease in binding affinity was observed (as compared to **27**) for both smaller substitutions (4-fluoro and 4-chloro, compounds **25** and **26** respectively) and larger substitutions (4-iodo, 4-trifluoromethyl, and 4-isopropyl, compounds **28, 29**, and **37**, respectively). Similar to the trends observed for the 2- and 3-positions, electron withdrawing groups at the 4-position also displayed higher binding affinity than electron donating groups. A hydrogen bond donor at the 4-position also displayed good binding affinity (4-hydroxyl, compound **32**), and this affinity could be altered by conversion to the methyl ether (**34**), which manifested decreased affinity. Compound **35**, containing a nitrile group at the 4-position, also displayed enhanced Grp94 binding, which may be attributed to its electron withdrawing ability as well as its ability to serve as a hydrogen bond acceptor. As predicted by molecular modeling studies which clearly outlined the **A** and **B** pockets as important for binding, both the 2- and 3-substituted compounds (**8** and **17**, respectively) exhibited the greatest influence on Grp94 binding as compared to the 4-substituted derivatives (**27**).

Preliminary molecular modeling studies (Scheme 1) indicated that one explanation for the enhanced activity of the phenyl amide scaffold was due to its potential to π-stack with the electron-rich rings of Phe199 and Tyr200, suggesting that π-stacking with these residues could be enhanced by alteration of the electron density on the phenyl ring. Structure-activity relationships at the 2-, 3-, and 4-positions supported this hypothesis as decreased electron density (via electron withdrawing groups) led to enhanced binding. Further validation of this hypothesis prompted the introduction of heteroatoms into the aromatic ring to enhance these π-stacking interactions.

Investigation of the influence that electron withdrawing groups exhibit led to a series heterocycles that exhibited decreased electron density within the aromatic ring. Sulfur containing 5-membered heterocycles (**46–48**) were synthesized to represent a ring similar in size as the corresponding 6-membered analogs (**38–45**), while manifesting some electron deficiency. As described previously, these analogs were generated by an EDCI-mediated coupling of TBS-protected acid **1** with corresponding amines **38a–48a**, followed by silyl-deprotection to afford the desired amides, **38–48**. Evaluation of the pyridine analogs showed that a nitrogen atom at the 2-position (**38**) resulted in the highest binding affinity, followed

by the 3- (**39**) and 4-incorporation (**40**), respectively (as shown in Figure 6). Molecular modeling studies suggest this trend was due at least in part by the ability of the nitrogen atom to project towards the open channel, while simultaneously maintaining optimal orientation for π-stacking with Phe199 and Tyr200. However, when the nitrogen was moved to the 3-position (**40**), nitrogen is shifted towards the channel, resulting in less favorable π-stacking interactions. The 4-pyridine derivative (**40**) demonstrated the lowest binding affinity due to its inability to access the open channel, and instead was forced into unfavorable interactions with the hydrophobic binding pocket of **B**. Pyridazine **42** was prepared to determine whether the incorporation of 2- and 3-containing nitrogen atoms could simultaneously exist while providing π-π interactions. Unfortunately **42** did not improve binding affinity, suggesting that the inclusion of a nitrogen atom at the meta-position is not favored. Subsequent analogs that contained the 2-pyridine nitrogen and other nitrogen locations (**41–45**, Figure 6) were explored, but unfortunately, did not improve affinity. In contrast, thiazole **46** and thiadiazoles **47** and **48** displayed good binding affinity and reinforced the importance of nitrogen incorporation at the 2-position.

An understanding of this scaffold's ability to selectively bind Grp94 required binding affinity evaluation to another isoform, Hsp90α. As shown in Figure 8, phenyl amide **2** did not demonstrate selectivity for Grp94 (~1:1), illustrating the need to optimize this scaffold for greater selectivity. However, substitution at the 2-, 3-, and 4-positions on the phenyl ring (compounds **8, 17**, and **27** respectively) did enhance selectivity for Grp94. Specifically, compound **27** showed the greatest selectivity (~27-fold at 25 μM), indicating the importance of substituents at the 4-position for selective inhibition, while **8** and **17** manifested 8- and 25-fold selectivity, respectively. It was also observed that heterocycles **38, 46** and **47** exhibited selectivity, albeit to a lesser extent than **8, 17**, and **27**. In an effort to further improve Grp94-selective binding, tertiary amides **49–53** were developed. These compounds were designed to enhance isomerization to the *cis*-amide conformation, by making the *cis*-conformation lower in energy, which appears preferred for Grp94-inhibition (Figure 1). Compounds **49, 50** and **53** were prepared by an EDCI-mediated coupling of TBS-protected acid **1** with anilines **49a, 50a**, and **53a**, followed by silyl-deprotection to afford the desired amides, **49, 50**, and **53**. **51** and **52** required an alternative method for their preparation. Compound **51** was generated by conversion of the benzyl-protected acid **1a** to the corresponding acid chloride, followed by coupling with aniline **51a** and subsequent debenzylation to afford desired amide **51** (Figure 7). Compound **52** was prepared by catalyst-mediated coupling of aldehyde **1b** with nitrosobenzene, followed by silyl-deprotection to afford amide **52** (Figure 7).[35] Unfortunately, compounds **49–51** and **53** exhibited little to no improvement in Grp94-selectivity (Figure 8), while simultaneously manifesting decreased binding affinities (Figures 7 and 8). In contrast, compound **52**, which contains an *N*-hydroxyl, demonstrated a significant increase in selectivity, however, at the consequence of lower affinity (Figures 7 and 8).

Further optimization of this scaffold was pursued to develop more potent and selective Grp94 inhibitors by combining the features identified above to produce **54–65**, which contain the phenyl amide, an ortho-pyridine, a thiazole, or a thiadiazole ring along with substitution patterns based on earlier studies (Figure 9). These compounds were also

synthesized by the EDCI-mediated coupling of acid **1** with anilines **54a–65a**. Subsequent silyl-deprotection of the resulting amides afforded **54–65**. Unfortunately, **54–58, 60, 61**, and **63–65** were unable to exhibit Grp94 binding affinity similar to **8, 17, 27** or **38**. Some of the compounds (**60, 61**, and **63**) exhibited a slight enhancement for Grp94 selectivity, but also demonstrated lesser affinity. However, **58, 59** and **62** demonstrated a high Grp94 binding affinity (≤1% tracer bound), while also manifesting good selectivity (4–18% tracer bound for Hsp90α). Despite these characteristics, compounds **54–65** did not manifest greater binding affinity or selectivity for Grp94 than previously prepared analogs.

Compounds **8, 17, 27, 38, 46** and **47** were evaluated for determination of their respective K_d values for Grp94 binding. K_d's were determined in a manner similar to the 25 μM fluorescence polarization screen, wherein compounds were incubated with Grp94 and FITC-GDA for 24 h at increasing concentrations. From the data, the K_d values for **8, 17, 27, 38, 46**, and **47** were determined as shown in Table 1. In accord with earlier studies, substitutions at the 2- and 4-positions (**8** and **27**, respectively) manifested better activity than the 3-position (**17**). The importance of a nitrogen atom at the 2-position was also confirmed as **38** manifested the highest affinity (0.82 μM), while both **46** and **47** also displayed less affinity (1.08 μM and 1.54 μM, respectively). Compounds **38** and **46** manifested the highest affinity for Grp94, and therefore were used in subsequent cell-based assays.

Inhibition of Migration and Proliferation of MDA-MB-231 cells

Inhibition of Grp94 has been linked to decreased metastasis, migration and proliferation in the highly metastatic breast cancer cell lines, MDA-MB-231 and ROS-resistant MCF-7.[20] Specifically, silencing Grp94 expression caused almost complete inhibition of migration as well as a signficant decrease in proliferation of the highly aggressive metastatic breast cancer cell line, MDA-MB-231.[20] While compounds **38** and **46** manifested modest anti-proliferative activities against MDA-MB-231 cells (**38**: IC_{50}=12 μM, **46**: IC_{50}=16 μM), they did demonstrate potent anti-migratory properties against the same cell line. This was determined by employing a wound healing assay where a monolayer of cells was grown in a 12-well plate format. In each well, two wounds were created in which cells can migrate and heal the wound. Migration was recorded at 0 h, 16 h, and 24 h using a digital camera mounted microscope. In addition, each compound was tested at 2.5 μM (Figure 10) up to 25 μM (Supporting Information, Figures S1–S2) where they demonstrated no cytotoxicity. The results at 2.5 μM are shown in Figure 10.

Compounds **38** and **46** were evaluated in this assay as they manifested the most potent (K_d values, Table 1) Grp94 inhibition while also manifesting good selectivity for Grp94 binding (Figure 8). As shown in Figure 10, they inhibited cell migration consistent with Grp94 inhibition, which was also in accord with prior studies by Verrax and coworkers[20], wherein they showed that Grp94 knockdown led to migratory inhibition of MDA-MB-231 cells. The ability of these compounds to inhibit migration mirrored the trend observed in the fluorescence polarization assay, where compound **38** manifested a greater anti-migratory effect than compound **46**. The anti-migratory effect of these compounds was determined to be dose-dependent (Supporting Information, Figures S1 and S2). Ultimately, the wound-

healing assay illustrates the potential for Grp94-inhibitors to be used in the treatment of highly metastatic breast cancers, while manifesting minimal toxicity.

Compounds **38** and **46** demonstrated the ability to bind Grp94 in MDA-MB-231 cells. The anti-Grp94 (9G10) antibody recognizes the open conformation of Grp94, and when an inhibitor is bound to this region, Grp94 switches to the closed conformation. Therefore, the 9G10 antibody does not recognize Grp94 bound to an inhibitor.[26,37] Compounds **38** and **46** demonstrated a dose-dependent effect by inducing a conformational change in Grp94, and thus, prevented the 9G10 antibody from recognizing and immunoprecipitating Grp94 from MDA-MB-231 cells (as shown in Figure 11). These findings correspond well with the observed anti-proliferative and anti-migratory concentrations, indicating these effects parallel Grp94-inhibition.

Previous studies have shown that Grp94-inhibition decreases insulin-like growth factor-II (IGF-II) secretion, which also plays an important role in the proliferation and migration of certain cancers.[26,51,52] Compounds **38** and **46** decreased secretion of the Grp94-dependent client protein, IGF-II, as shown in Figure 12. The dramatic decrease in IGF-II secretion was observed at concentrations that parallel the concentrations needed to exhibit anti-migratory activity.

Compounds **38** and **46** also demonstrated selective Grp94-inhibition by Western blot analysis of Hsp90 client proteins Akt and Cyclin D1 from MDA-MB-231 cell lystates (Figure 13). Degradation of Hsp90-dependent cytosolic clients, Akt and Cyclin D1, was not observed at a high concentration of compound **38** (60 μM), indicating other Hsp90 isoforms were not affected at the concentration needed to exhibit anti-migratory activity (2.5–25 μM). Compound **46** demonstrated modest client-protein degradation at 80 μM, however, this effect was observed at concentrations significantly higher than the concentration needed for anti-migratory activity. This finding along with the observed effects of utilizing the 9G10 antibody (Figure 11) and decreased IGF-II secretion (Figure 12) indicate these compounds inhibit Grp94 at concentrations relevant to the observed anti-migratory activity.

Anti-proliferative effect on RPMI 8226 cells

Recently, elevated levels of Grp94 were linked to the accelerated proliferation of multiple myeloma cells,[22–24] identifying Grp94 as a potential therapeutic target for the treatment of myeloma.[25] The RPMI 8226 multiple myeloma cell line was shown to be particularly sensitive to Grp94 inhibition, which prompted investigation of compounds **38** and **46** for their anti-proliferative activity against this cell line.

As anticipated, the two most potent compounds for binding Grp94 (Table 1) also exhibited potent anti-proliferative properties against the RPMI 8226 cell line (IC_{50} <10 μM). Interestingly, **38** displayed a slightly lower anti-proliferative effect (9.12 μM) than **46** despite its superior binding affinity. These compounds were then evaluated for their ability to selectively inhibit Grp94 in RPMI 8226 cells in a similar fashion seen for MDA-MB-231 cells.

Compounds **38** and **46** did demonstrate an ability to bind Grp94 in RPMI 8226 cells in a dose-dependent manner. This was first determined by use of the 9G10 antibody to recognize Grp94 in immunoprecipitated RPMI8226 cell lysates treated with compounds **38** and **46** (Figure 14). These data indicate that compounds **38** and **46** bind Grp94 at concentrations needed to inhibit the proliferation of RPMI 8226 cells.

Compounds **38** and **46** also decreased secretion of the Grp94-dependent client protein, IGF-II; at concentrations similar to the observed anti-proliferative activity manifested by both compounds (Figure 15). Along with the use of the 9G10 antibody (Figure 14), this data also suggests that the observed anti-proliferative activity of compounds **38** and **46** against RPMI 8226 cells is attributed to the inhibition of Grp94 in RPMI 8226 cells.

Compounds **38** and **46** also demonstrated that their anti-proliferative activities are likely due to selective Grp94 inhibition. This was illustrated by the inability of compound **38** to degrade Hsp90 client-proteins Akt and cyclin D1 (Figure 16) at concentrations above and below its respective anti-proliferative IC_{50} value. Compound **46** demonstrated modest client-protein degradation at concentrations five-fold higher than its IC_{50}, indicating a slightly lower selectivity for Grp94. However, this data does indicate that compounds **38** and **46** inhibit Grp94 in RPMI 8226 cells, which results in their anti-proliferative activity. The ability of this scaffold to selectively inhibit Grp94 and manifest anti-proliferative activity against the RPMI 8226 multiple myeloma cell line demonstrates the therapeutic potential of Grp94 inhibition for the treatment of these cancers.

Conclusion

Using the previously reported co-crystal structure of RDA bound to Grp94, a series of RDA analogs were designed, synthesized, and evaluated for their ability to inhibit Grp94. A comprehensive SAR study of this scaffold indicated several key features necessary for selective inhibition of Grp94 (Figure 17). Initial optimization of the linker led to the identification of phenyl amide, **2**, manifesting the highest Grp94 affinity (blue, Figure 17). This finding demonstrated both the importance of a short linker, as well as the presence of an aromatic ring for π-stacking interactions. Substituents at the 2- and 4-positions (pink and green, Figure 17) of the phenyl amide demonstrated increased Grp94 binding affinity and selectivity, with chlorine and bromine substituents identified as optimal (Table 1, compounds **8** and **27**, respectively). Substitution at the 3-position (orange, Figure 17) also proved important; however, both potency and selectivity were decreased relative to substitutions at the 2- and 4-positions (Table 1, compound **17**). In contrast, modifications to the 4-position resulted in the greatest effect on selectivity, as most substituents at this position manifested enhanced selectivity. Decreasing the electron density of the aromatic ring via the introduction of heteroatoms (**38, 46**, and **47**) not only increased binding affinity, but also increased selectivity. However, this finding was specific to the incorporation of a nitrogen atom at the 2-position (Figure 6). The 2-pyridine ring was successfully incorporated with the 4-bromine or 3-chlorine derivative to provide potent and selective Grp94-inhibitors. Subsequent *in vitro* analysis of **38** and **46** further validated the therapeutic potential for Grp94 inhibitors as well as validated selective Grp94-inhibition. The ability of these compounds to inhibit Grp94 was correlative with their anti-migratory activity against the

highly metastatic breast cancer cell line, MDA-MB-231, as well as anti-proliferative activity against the multiple myeloma cell line, RPMI 8226.

General Experimental Methods

Fluorescence Polarization

Assay buffer (25 μL, 20 mM HEPES pH 7.3, 50 mM KCl, 5 mM $MgCl_2$, 1 mM DTT, 20 mM Na_2MoO_4, 0.01% NP-40, and 0.5 mg/mL BGG) containing desired compound or GDA were plated in 96-well plates (black well, black bottom) at the indicated final concentrations in DMSO (1% DMSO final concentration).[32] Recombinant cGrp94 and FITC-GDA were then added (10 and 6 nM, respectively). Plates were incubated with rocking for 24 h at 4°C. Fluorescence was read using excitation and emission filters of 485 and 528 nm, respectively. Percent FITC-GDA bound was determined by using the DMSO millipolarization unit (mP) as the 100% bound value and the mP value of free FITC-GDA as the 0% bound value. K_d values were calculated from separate experiments performed in triplicate using GraphPad Prism.

Anti-proliferation Assays

RPMI 8226 and MDA-MB-231 cells were maintained in RPMI1640 (Cellgro) and DMEM (Cellgro), respectively, supplemented with nonessential amino acids , L-glutamine (2 mM), streptomycin (500 μg/mL), penicillin (100 units/mL) and 10% FBS. Cells were grown to confluence in a humidified atmosphere (37°C, 5% CO_2), seeded (2000/well, 100 μL) in 96-well plates, and allowed to attach overnight. Compound at varying concentrations in DMSO (1% DMSO final concentration) was added, and cells were returned to the incubator for 72 h. After 72 h, the number of viable cells was determined using an MTS/PMS cell proliferation kit (Promega) per the manufacturer's instructions. Cells incubated in 1% DMSO were use as 100% proliferation, and values were adjusted accordingly. IC_{50} values were calculated from separate experiments performed in triplicate using GraphPad Prism.

Wound-Healing Assay

Cells were grown to confluence in a humidified atmosphere (37°C, 5% CO_2), seeded (200000/well, 1 mL) in 12-well plates, and allowed to grow to a confluent monolayer (24 h) at 37°C and 5% CO_2. Each well was then scratched with a 200 μL sterile pipet tip, photographed with an Olympus IX-71 microscope (60x objective, time=0 h), the respective compound solutions (2.5 μL, final DMSO concentration is 0.25%) were added, and the plates were placed back in the incubator. Cell migration was recorded after 16 and 24 h of incubation with compound via photographs taken by the Olympus IX-71 microscope. All experiments were run in quadruplicate on two different days.

Western Blotting

MDA-MB-231 and RPMI 8226 cells were plated in 6-well plates and treated with high and low concentrations of compounds **38** and **46**, as well as 15 μM RDC in DMSO (0.25% DMSO final concentration), or DMSO only for 24 h. Cells were harvested in cold PBS and lysed in mammalian protein extraction reagent (MPER, Pierce) and protease inhibitors (Roche) on ice for 15 min. Lysates were clarified at 15,000 rpm for 15 min at 4°C. Protein

concentrations were determined with the Pierce BCA assay kit per the manufacturer's instructions. Equal amounts of protein (20 μg) were electrophoresed under reducing conditions, transferred to a PVDF membrane, and immunoblotted with the corresponding specific antibodies. The corresponding amount of media necessary to maintain equal actin levels was also electrophoresed under reducing conditions, transferred to a PVDF membrane, and immunoblotted with the IGF-II antibody. Membranes were incubated with an appropriate horseradish peroxidase-labeled secondary antibody, developed with chemiluminescent substrate, and visualized.

Grp94 Immunoprecipitation

Detergent lysates of the indicated cells were immunoprecipitated with 9G10 monoclonal anti-Grp94 (Enzo Life Sciences) followed by protein G-MagBeads (GenScript) as previously described.[37]

Molecular Modeling

Surflex-Dock in Sybyl v8.0 was used for molecular modeling and docking studies. The co-crystal structure of RDA bound to Grp94 was utilized for all docking experiments.[30] The docked molecules were locked into the *cis*-amide conformation and utilized with 10 different starting conformations while rotation of the rotatable bonds was unrestricted. Visual interpretation and figure preparation were then carried out in Pymol.

Chemistry General

^{1}H NMR were recorded at 400 or 500 MHz (Bruker DRX-400 Bruker with a H/C/P/F QNP gradient probe) spectrometer and ^{13}C NMR spectra were recorded at 125 MHz (Bruker DRX 500 with broadband, inverse triple resonance, and high resolution magic angle spinning, HR-MA probe spectrometer); chemical shifts are reported in δ (ppm) relative to the internal chloroform-*d* ($CDCl_3$, 7.27 ppm). FAB (HRMS) spectra were recorded with a LCT Premier (Waters Corp., Milford, MA). The purity of all compounds was determined to be >95% purity as determined by ^{1}H NMR and ^{13}C NMR spectra, unless otherwise noted. The most active five compounds were verified for >95% purity by HPLC analyses. TLC was performed on glass backed silica gel plates (Uniplate) with spots visualized by UV light. All solvents were reagent grade and, when necessary, were purified and dried by standard methods. Concentration of solutions after reactions and extractions involved the use of a rotary evaporator operating at reduced pressure.

General Amide Formation for Compounds 2–50 and 53–65

To a solution of acid **1** (0.05 mmol), EDCI·HCl (0.12 mmol), and pyridine (0.13 mmol) in CH_2Cl_2 (1 mL) was added the corresponding aniline (0.1 mmol) and stirred at room temperature under Ar overnight. Upon complete consumption of acid **1**, the solvent was removed in vacuo and redissolved in THF (1 mL). The reaction mixture was then treated with TBAF (0.2 mmol) and stirred for 30 min, and upon completion saturated aqueous NH_4Cl was added and extracted 3x with EtOAc. The combined organic layers were then dried over Na_2SO_4, filtered, and concentrated *in vacuo* to give a crude oil. The residue was purified via flash chromatography (SiO_2, 49:1, CH_2Cl_2:MeOH) to afford the desired amide.

methyl 3-chloro-4,6-dihydroxy-2-(3-oxo-3-(phenylamino)propyl)benzoate (2)— 15 mg, 86% yield, white solid. ^{1}H NMR (400 MHz, $CDCl_3$): δ 11.23 (s, 1 H), 7.53 (d, *J* = 7.91 Hz, 2 H), 7.34 (t, *J* = 7.66 Hz, 2 H), 7.12 (t, *J* = 7.36 Hz, 1 H), 6.59 (s, 1 H), 6.33 (s, 1 H), 3.97 (s, 3 H), 3.50 (dd, *J* = 5.76, 10.15 Hz, 2 H), 2.66–2.59 (m, 2 H). ^{13}C NMR (125 MHz, $CDCl_3$): δ = 170.43, 169.99, 162.91, 156.28, 141.66, 137.73, 129.10 (2 C), 124.40, 119.72 (2 C), 113.92, 106.81, 102.94, 52.75, 36.73, 28.81. HRMS (FAB) *m/z* [M+Na^+] for $C_{17}H_{16}ClNO_5Na$: 372.0609, found 372.0609.

methyl 2-(3-(benzylamino)-3-oxopropyl)-3-chloro-4,6-dihydroxybenzoate (3)— 30 mg, 83% yield, white solid. ^{1}H NMR (500 MHz, $CDCl_3$): δ 7.32 – 7.21 (m, 5H), 6.44 (s, 1H), 4.40 (d, *J* = 4.7 Hz, 2H), 3.86 (s, 3H), 3.44 – 3.29 (m, 2H), 2.50 – 2.33 (m, 2H). ^{13}C NMR (125 MHz, $CDCl_3$) δ 171.98, 170.68, 162.51, 157.03, 141.87, 138.12, 127.81, 127.60, 114.22, 106.34, 102.63, 52.53, 49.78, 43.73, 35.65, 28.92. HRMS (FAB) *m/z* [M+Na^+] for $C_{18}H_{18}ClNO_5Na$: 386.0874; found, 386.0877.

methyl 3-chloro-4,6-dihydroxy-2-(3-oxo-3-(phenethylamino)propyl)benzoate (4)—17 mg, 90% yield, white solid. ^{1}H NMR (400 MHz, $CDCl_3$): δ 11.29 (s, 1 H), 7.32 (dd, *J* = 6.63, 8.10 Hz, 2 H), 7.26–7.23 (m, 1 H), 7.22–7.17 (m, 2 H), 6.57 (s, 1 H), 5.48 (t, *J* = 5.95 Hz, 1 H), 3.91 (s, 3 H), 3.56 (q, *J* = 6.58 Hz, 2 H), 3.40–3.34 (m, 2 H), 2.84 (t, *J* = 6.84 Hz, 2 H), 2.41–2.35 (m, 2 H). ^{13}C NMR (125 MHz, $CDCl_3$): δ 171.92, 170.64, 162.90, 156.43, 141.74, 138.72, 128.77, 128.71, 126.63, 113.90, 106.64, 102.80, 52.58, 40.63, 35.81, 35.61, 29.05. HRMS (FAB) *m/z* [M+Na^+] for $C_{19}H_{20}ClNO_5Na$: 400.0922, found 400.0931.

methyl 3-chloro-4,6-dihydroxy-2-(3-oxo-3-(2-phenylhydrazinyl)propyl)benzoate (5)—17 mg, 94% yield, orange solid. ^{1}H NMR (400 MHz, CD_3OD, major conformer): δ 7.23–7.13 (m, 2 H), 6.83–6.74 (m, 3 H), 6.41 (s, 1 H), 3.92 (s, 3 H), 3.36–3.28 (m, 2 H), 2.59–2.53 (m, 2 H); ^{13}C NMR (125 MHz, CD_3OD, major conformer): δ 174.8, 171.6, 161.5, 159.0, 150.0, 142.1, 130.2, 130.0, 121.0, 115.0, 114.1, 113.3, 109.5, 103.2, 52.9, 34.3, 29.1. HRMS (FAB) *m/z* [M+Na^+] for $C_{17}H_{17}ClN_2O_5Na$: 387.0724; found, 387.0723.

methyl 3-chloro-2-(3-(cyclohexylamino)-3-oxopropyl)-4,6-dihydroxybenzoate (6)—33 mg, 88% yield, white solid. ^{1}H NMR (500 MHz, $CDCl_3$) δ 6.41 (s, 1H), 3.89 (s, 3H), 3.68 (s, 1H), 3.40 – 3.24 (m, 2H), 2.40 – 2.26 (m, 2H), 1.91 – 1.76 (m, 2H), 1.64 (dt, *J* = 13.8, 3.8 Hz, 2H), 1.61 – 1.52 (m, 1H), 1.39 – 1.25 (m, 2H), 1.07 (ddd, *J* = 19.2, 9.8, 3.9 Hz, 3H). ^{13}C NMR (125 MHz, $CDCl_3$) δ 171.44, 170.78, 162.49, 157.48, 142.07, 114.43, 106.04, 102.51, 52.46, 49.40, 48.22, 35.90, 33.07, 28.92, 25.46, 24.83. HRMS (FAB) *m/z* [M+Na^+] for $C_{17}H_{22}ClNO_5Na$: 378.1187; found, 378.1167.

methyl 3-fluoro-2-(3-((2-chlorophenyl)amino)-3-oxopropyl)-4,6-dihydroxybenzoate (7)—15 mg, 81% yield, white solid. ^{1}H NMR (500 MHz, $CDCl_3$) δ 11.19 (s, 1H), 8.49 – 8.00 (m, 1H), 7.34 (s, 1H), 7.12 – 6.97 (m, 3H), 6.53 (s, 1H), 6.05 (s, 1H), 3.91 (s, 3H), 3.49 – 3.37 (m, 2H), 2.67 – 2.57 (m, 2H).^{13}C NMR (125 MHz, $CDCl_3$) δ 170.45, 169.98, 163.02, 156.23, 141.37, 124.71, 124.68, 124.37, 124.31, 121.60, 114.87,

114.72, 113.86, 106.81, 102.99, 52.73, 36.80, 28.83. HRMS (FAB) *m/z* [M+Na^+] for $C_{17}H_{15}ClFNO_5Na$: 390.0521; found, 390.0547.

methyl 3-chloro-2-(3-((2-chlorophenyl)amino)-3-oxopropyl)-4,6-dihydroxybenzoate (8)—14 mg, 73% yield, white solid. ^{1}H NMR (500 MHz, $CDCl_3$) δ 11.22 (s, 1H), 8.36 (d, *J* = 8.3 Hz, 1H), 7.61 (s, 1H), 7.31 (dd, *J* = 8.0, 1.5 Hz, 1H), 7.26 – 7.21 (m, 1H), 7.02 – 6.97 (m, 1H), 6.53 (s, 1H), 3.91 (s, 4H), 3.54 – 3.32 (m, 2H), 2.76 – 2.47 (m, 3H).^{13}C NMR (125 MHz, $CDCl_3$) δ 170.49, 163.08, 156.23, 141.30, 134.49, 129.04, 127.85, 124.68, 121.47, 113.86, 106.83, 103.00, 52.75, 37.03, 28.90. HRMS (FAB) *m/z* [M+Na^+] for $C_{17}H_{15}Cl_2NO_5Na$: 406.0225; found, 406.0246.

methyl 2-(3-((2-bromophenyl)amino)-3-oxopropyl)-3-chloro-4,6-dihydroxybenzoate (9)—16.3 mg, 76% yield, pale yellow solid. ^{1}H NMR (500 MHz, $CDCl_3$) δ 11.25 (s, 1H), 8.49 – 7.19 (m, 7H), 6.93 (td, *J* = 7.7, 1.4 Hz, 1H), 6.53 (s, 1H), 6.13 (s, 1H), 3.91 (s, 3H), 3.53 – 3.36 (m, 2H), 2.64 (t, *J* = 8.3 Hz, 2H).^{13}C NMR (125 MHz, $CDCl_3$) δ 170.54, 170.04, 163.07, 156.29, 141.26, 135.54, 132.27, 128.50, 125.26, 121.80, 113.89, 113.18, 106.80, 103.01, 52.79, 37.05, 27.08. HRMS (FAB) *m/z* [M+Na^+] for $C_{17}H_{15}BrClNO_5Na$: 449.9720; found, 449.9767.

methyl 3-chloro-4,6-dihydroxy-2-(3-((2-iodophenyl)amino)-3-oxopropyl)benzoate (10)—18.2 mg, 77% yield, pale yellow solid. ^{1}H NMR (500 MHz, $CDCl_3$) δ 11.27 (s, 1H), 8.21 (d, *J* = 8.2 Hz, 1H), 7.77 – 7.23 (m, 3H), 6.82 – 6.78 (m, 1H), 6.53 (s, 1H), 6.03 (s, 1H), 3.92 (s, 3H), 3.51 – 3.37 (m, 3H), 2.72 – 2.52 (m, 3H). ^{13}C NMR (125 MHz, $CDCl_3$) δ 170.58, 163.13, 156.24, 141.26, 138.84, 138.04, 129.38, 126.07, 121.88, 113.88, 106.85, 103.01, 52.84, 37.05, 28.97. HRMS (FAB) *m/z* [M+Na^+] for $C_{17}H_{15}ClINO_5Na$: 497.9581; found, 497.9593.

methyl 3-chloro-4,6-dihydroxy-2-(3-oxo-3-((2-(trifluoromethyl)phenyl)amino)propyl)benzoate (11)—33 mg, 79% yield, white amorphous solid: ^{1}H NMR (400 MHz, $CDCl_3$-MeOD) δ 6.87 (d, *J* = 1.4 Hz, 1H), 6.84 (d, *J* = 1.4 Hz, 1H), 6.41 (s, 1H), 6.08 (d, *J* = 3.1 Hz, 1H), 5.84 (dd, *J* = 3.0, 1.3 Hz, 1H), 4.88 (s, 2H), 3.84 (s, 3H), 3.49 – 3.41 (m, 2H), 3.02 – 2.92 (m, 2H); ^{13}C NMR ($CDCl_3$+CH_3OH, 125 MHz): δ 171.0, 162.2, 158.3, 153.1, 147.3, 147.1, 141.9, 126.7, 119.7, 114.9, 109.7, 106.5, 102.6, 52.6, 42.7, 30.9, 26.2. (FAB) *m/z* [M + H^+] for $C_{18}H_{16}ClF_3NO_5$: 418.0669; found, 418.0658.

methyl 3-chloro-4,6-dihydroxy-2-(3-((2-hydroxyphenyl)amino)-3-oxopropyl)benzoate (12)—23 mg, 63% yield, white amorphous solid: ^{1}H NMR (500 MHz, $(CD_3)_2CO$) δ 9.21 (br s, 1H), 7.49 (dd, *J* = 8.1, 1.6 Hz, 1H), 7.03 (td, *J* = 7.8, 1.6 Hz, 1H), 6.91 (dd, *J* = 8.1, 1.5 Hz, 1H), 6.82 (td, *J* = 7.7, 1.5 Hz, 1H), 6.52 (s, 1H), 3.96 (s, 3H), 3.54 – 3.37 (m, 2H), 2.87 – 2.74 (m, 2H); ^{13}C NMR (125 MHz, $(CD_3)_2CO$): δ 172.9, 171.3, 162.4, 158.7, 149.1, 142.8, 127.6, 126.5, 122.7, 120.6, 118.7, 114.9, 108.1, 103.2, 53.0, 36.3, 29.4; (FAB) *m/z* [M + H^+] for $C_{17}H_{16}ClNO_6$: 388.0563; found, 388.0563.

methyl 3-chloro-4,6-dihydroxy-2-(3-((2-methoxyphenyl)amino)-3-oxopropyl)benzoate (13)—14.5 mg, 77% yield, white solid. ^{1}H NMR (500 MHz,

$CDCl_3$) δ 11.40 (s, 1H), 8.41 (dd, *J* = 7.9, 1.7 Hz, 1H), 7.77 (s, 1H), 7.10 – 6.85 (m, 3H), 6.59 (s, 1H), 3.96 (s, 3H), 3.87 (s, 3H), 3.56 – 3.46 (m, 2H), 2.71 – 2.62 (m, 2H).^{13}C NMR (125 MHz, CD_3OD) δ 173.39, 171.67, 161.61, 158.99, 151.43, 142.28, 128.21, 126.10, 123.37, 121.46, 114.98, 111.74, 109.46, 103.16, 56.19, 52.83, 37.23, 29.40. HRMS (FAB) *m/z* [M+H] for C18H18ClNO6: 380.0901; found, 380.0920.

methyl 2-(3-((2-aminophenyl)amino)-3-oxopropyl)-3-chloro-4,6-dihydroxybenzoate (14)—7.5 mg, 41% yield, pale yellow solid. ^{1}H NMR (400 MHz, CD_3OD) δ 7.05 – 6.92 (m, 2H), 6.79 – 6.61 (m, 1H), 6.32 (d, *J* = 4.7 Hz, 1H), 3.84 (d, *J* = 5.2 Hz, 3H), 3.31 – 3.25 (m, 2H), 2.66 – 2.60 (m, 2H). ^{13}C NMR (125 MHz, CD_3OD) δ 173.77, 171.72, 161.58, 159.34, 143.21, 142.29, 128.24, 127.13, 125.21, 119.62, 118.61, 115.21, 109.28, 103.28, 52.91, 36.45, 29.33. HRMS (FAB) *m/z* [M+Na^+] for $C_{17}H_{17}ClN_2O_5Na$: 387.0724; found, 387.0744.

methyl 3-chloro-4,6-dihydroxy-2-(3-oxo-3-(o-tolylamino)propyl)benzoate (15)—10 mg, 25% yield, white powder. ^{1}H NMR (400 MHz, $CDCl_3$): δ 11.19 (s, 1 H), 7.87 (d, *J* = 8.0 Hz, 1 H), 7.28–7.19 (m, 2 H), 7.19–7.07 (m, 2 H), 6.67 (bs, 1 H), 6.60 (s, 1 H), 4.00 (s, 3 H), 3.60–3.48 (m, 2 H), 2.78–2.62 (m, 2 H), 2.29 (s, 3 H); ^{13}C NMR (125 MHz, $CDCl_3$ and CD_3OD): δ 170.8, 170.5, 161.9, 157.8, 141.9, 135.3, 130.4, 129.5, 126.6, 125.3, 123.4, 114.6, 106.0, 102.4, 52.4, 36.3, 28.9, 17.6. HRMS (FAB) *m/z* [M+Na^+] for $C_{18}H_{18}ClNO_5Na$: 386.0771; found, 386.0769.

methyl 3-chloro-2-(3-((3-fluorophenyl)amino)-3-oxopropyl)-4,6-dihydroxybenzoate (16)—27 mg, 74% yield, white amorphous solid: ^{1}H NMR (500 MHz, $(CD_3)_2CO$) δ 9.38 (br s, 1H), 7.86 – 7.64 (m, 1H), 7.37 – 7.22 (m, 2H), 6.81 (ddt, *J* = 9.1, 6.3, 2.6 Hz, 1H), 6.51 (s, 1H), 3.95 (s, 3H), 3.57 – 3.20 (m, 2H), 2.84 – 2.52 (m, 2H); ^{13}C NMR(125 MHz, $(CD_3)_2CO$): δ 171.3, 164.7, 162.8, 162.3, 158.6, 143.0, 142.1, 131.0, 130.9, 115.5, 110.4, 108.2, 106.9, 103.2, 52.9, 36.8, 28.8; HRMS (FAB) *m/z* [M + H^+] for $C_{17}H_{15}ClFNO_5$: 368.0701; found, 368.0701.

methyl 3-chloro-2-(3-((3-chlorophenyl)amino)-3-oxopropyl)-4,6-dihydroxybenzoate (17)—30 mg, 78% yield, white amorphous solid: ^{1}H NMR (500 MHz, $(CD_3)_2CO$) δ 9.33 (s, 1H), 8.06 – 7.85 (m, 1H), 7.49 (ddd, *J* = 8.2, 2.1, 1.0 Hz, 1H), 7.31 (t, *J* = 8.1 Hz, 1H), 7.08 (ddd, *J* = 7.9, 2.1, 0.9 Hz, 1H), 6.51 (s, 1H), 3.95 (s, 3H), 3.69 – 3.33 (m, 2H), 2.85 – 2.53 (m, 2H); ^{13}C NMR(125MHz. $(CD_3)_2CO$): δ 171.3, 171.3, 162.3, 158.6, 143.0, 141.8, 134.7, 131.0, 123.8, 119.8, 118.1, 114.8, 108.2, 103.2, 52.9, 36.8, 28.8; HRMS (FAB) *m/z* [M – H^-] for $C_{17}H_{14}Cl_2NO_5$: 382.0249; found, 382.0237.

methyl 2-(3-((3-bromophenyl)amino)-3-oxopropyl)-3-chloro-4,6-dihydroxybenzoate (18)—27 mg, 74% yield, white amorphous solid: ^{1}H NMR (500 MHz, $(CD_3)_2CO$) δ 9.32 (s, 1H), 8.10 (q, *J* = 1.6 Hz, 1H), 7.66 – 7.46 (m, 1H), 7.38 – 7.15 (m, 2H), 6.51 (s, 1H), 3.95 (s, 3H), 3.60 – 3.33 (m, 2H), 2.73 – 2.61 (m, 2H). ^{13}C NMR (125 MHz, $(CD_3)_2CO$) δ 171.32, 171.26, 158.63, 142.99, 141.93, 131.31, 126.77, 122.77, 122.70, 122.62, 118.63, 118.54, 114.81, 108.21, 103.18, 52.93, 36.81, 36.76, 28.84; HRMS (FAB) *m/z* [M + Na^+] for $C_{17}H_{15}ClBrNO_5Na$: 449.9720; found, 449.9720.

methyl 3-chloro-4,6-dihydroxy-2-(3-oxo-3-((3-(trifluoromethyl)phenyl)amino)propyl)benzoate (19)—34 mg, 81% yield, white amorphous solid: ^{1}H NMR (400 MHz, $CDCl_3$) δ 7.85 (s, 1H), 7.77 – 7.65 (m, 1H), 7.39 (t, *J* = 7.9 Hz, 1H), 7.32 – 7.28 (m, 1H), 6.41 (d, *J* = 0.7 Hz, 1H), 5.27 (d, *J* = 0.7 Hz, 1H), 3.91 (d, *J* = 0.7 Hz, 3H), 3.50 – 3.39 (m, 2H), 2.67 – 2.45 (m, 2H); ^{13}C NMR (125 MHz, $CDCl_3$): δ 170.7, 161.8, 158.0, 147.6, 141.6, 136.8, 136.5, 129.4, 126.4, 126.0, 125.1, 124.5, 120.1, 106.0, 102.4, 52.3, 30.7, 26.1; HRMS (FAB) *m/z* [M + H^+] for $C_{18}H_{16}ClF_3NO_5$: 418.0669; found, 418.0661.

methyl 2-(3-([1,1'-biphenyl]-3-ylamino)-3-oxopropyl)-3-chloro-4,6-dihydroxybenzoate (20)—35 mg, 72% yield, white amorphous solid: ^{1}H NMR (500 MHz, $(CD_3)_2CO$) δ 8.10 – 8.01 (m, 1H), 7.66 (tdd, *J* = 6.3, 2.1, 1.0 Hz, 3H), 7.52 – 7.44 (m, 2H), 7.44 – 7.33 (m, 3H), 6.52 (s, 1H), 3.97 (s, 3H), 3.63 – 3.36 (m, 2H), 2.73 – 2.56 (m, 2H); ^{13}C NMR(125 MHz, $(CD_3)_2CO$): δ 143.2, 130.1, 129.7, 128.3, 127.7, 122.6, 118.9, 118.5, 103.1, 52.9, 36.8, 29.0; . HRMS (FAB) *m/z* [M +Na^+] for $C_{23}H_{20}ClNO_5Na$: 448.0928; found, 448.0927.

methyl 3-chloro-4,6-dihydroxy-2-(3-((3-hydroxyphenyl)amino)-3-oxopropyl)benzoate (21)—16 mg, 88% yield, off-white solid. . ^{1}H NMR (400 MHz, CD_3OD): δ 7.16 (t, *J* = 2.27 Hz, 1 H), 7.06 (td, *J* = 2.36, 8.01 Hz, 1 H), 6.92 (dd, *J* = 2.70, 7.62 Hz, 1 H), 6.50 (dd, *J* = 2.47, 8.35 Hz, 1 H), 6.37 (s, 1 H), 3.86 (s, 3 H), 3.91 (s, 3 H), 3.32–3.25 (m, 2 H), 2.60 (ddt, *J* = 3.13, 7.38 Hz, 10.18, 2 H). ^{13}C NMR (125 MHz, CD_3OD): δ 173.26, 171.66, 161.48, 158.88, 142.34, 140.93, 130.50, 114.95, 114.93, 112.36, 112.09, 109.54, 108.40, 103.14, 52.87, 37.06, 29.09. HRMS (FAB) *m/z* [M+Na^+] for $C_{17}H_{16}ClNO_6Na$: 388.0558, found 388.0555.

methyl 3-chloro-4,6-dihydroxy-2-(3-((3-methoxyphenyl)amino)-3-oxopropyl)benzoate (22)—14.6 mg, 76% yield, white solid. ^{1}H NMR (500 MHz, $CDCl_3$) δ 11.15 (s, 1H), 7.30 – 7.11 (m, 3H), 6.92 – 6.58 (m, 2H), 6.52 (s, 1H), 6.25 (s, 1H), 3.90 (s, 3H), 3.75 (s, 3H), 3.46 – 3.37 (m, 2H), 2.58 – 2.51 (m, 2H).^{13}C NMR (126 MHz, $CDCl_3$) δ 170.82, 170.71, 162.10, 160.03, 157.67, 142.01, 139.24, 129.61, 114.59, 111.83, 109.92, 106.09, 105.39, 102.47, 55.27, 52.54, 36.41, 28.58. HRMS (FAB) *m/z* [M+Na^+] for $C_{18}H_{18}ClNO_6$: 402.0720; found, 402.0722.

methyl 2-(3-((3-aminophenyl)amino)-3-oxopropyl)-3-chloro-4,6-dihydroxybenzoate (23)—9 mg, 49% yield, pale yellow solid. ^{1}H NMR (400 MHz, $CDCl_3$) δ 7.12 – 7.05 (m, 1H), 7.01 (t, *J* = 8.0 Hz, 1H), 6.68 (dd, *J* = 7.8, 2.1 Hz, 1H), 6.44 – 6.26 (m, 2H), 3.87 (s, 3H), 3.38 (t, *J* = 8.4 Hz, 2H), 2.61 – 2.47 (m, 2H). ^{13}C NMR (125 MHz, $CDCl_3$) δ 170.50, 162.27, 157.40, 146.36, 141.98, 129.72, 114.46, 111.35, 110.11, 106.84, 106.20, 102.55, 52.57, 36.57, 29.69, 28.69. HRMS (FAB) *m/z* [M+Na^+] for $C_{17}H_{17}ClN_2O_5Na$: 387.0724; found, 387.0736.

methyl 2-(3-((3-acetamidophenyl)amino)-3-oxopropyl)-3-chloro-4,6-dihydroxybenzoate (24)—18 mg, 89% yield white solid. ^{1}H NMR (400 MHz, CD_3OD): δ 7.86 (t, *J* = 1.91 Hz, 1 H), 7.34–7.21 (m, 3 H), 6.40 (s, 1 H), 3.91 (s, 3 H), 3.36–3.32 (m, 2

H), 2.69–2.62 (m, 2 H), 2.12 (d, J = 1.77 Hz, 3 H). ^{13}C NMR (125 MHz, CD_3OD): δ 173.33, 171.69, 171.65, 161.43, 159.00, 142.26, 140.37, 140.33, 130.02, 116.94, 116.83, 114.97, 113.06, 109.58, 103.15, 52.84, 37.01, 29.04, 23.81. HRMS (FAB) *m/z* [M+Na^+] for $C_{19}H_{19}ClN_2O_6Na$: 428.0829, found 429.0824.

methyl 3-chloro-2-(3-((4-fluorophenyl)amino)-3-oxopropyl)-4,6-dihydroxybenzoate (25)—14.5 mg, 80% yield, white solid. ^{1}H NMR (500 MHz, $CDCl_3$) δ 11.28 (s, 1H), 7.89 (s, 1H), 7.50 (ddd, J = 9.4, 4.8, 2.4 Hz, 2H), 7.02 (t, J = 8.7 Hz, 2H), 6.50 (s, 1H), 3.96 (s, 3H), 3.52 – 3.44 (m, 2H), 2.65 – 2.56 (m, 2H). ^{13}C NMR (125 MHz, $CDCl_3$) δ 170.34, 169.85, 162.91, 160.34, 156.21, 141.58, 121.57, 121.50, 115.82, 115.64, 113.88, 106.86, 102.98, 52.73, 36.57, 28.79.HRMS (FAB) *m/z* [M+Na^+] for $C_{17}H_{15}ClFNO_5Na$: 390.0521; found, 390.0553.

methyl 3-chloro-2-(3-((4-chlorophenyl)amino)-3-oxopropyl)-4,6-dihydroxybenzoate (26)—13.8 mg, 72% yield, white solid. ^{1}H NMR (500 MHz, $CDCl_3$) δ 11.16 (s, 1H), 7.52 – 7.45 (m, 2H), 7.32 – 7.28 (m, 2H), 6.60 (s, 1H), 6.14 (s, 1H), 3.97 (s, 3H), 3.55 – 3.45 (m, 2H), 2.65 – 2.59 (m, 2H). ^{13}C NMR (125 MHz, $CDCl_3$) δ 170.45, 170.35, 162.39, 157.07, 141.80, 136.48, 129.09, 128.99, 120.94, 120.84, 114.29, 106.38, 102.70, 52.62, 36.48, 28.64.HRMS (FAB) *m/z* [M+Na^+] for $C_{17}H_{15}Cl_2NO_5Na$: 406.0225; found, 406.0234.

methyl 2-(3-((4-bromophenyl)amino)-3-oxopropyl)-3-chloro-4,6-dihydroxybenzoate (27)—15 mg, 70% yield, white solid. ^{1}H NMR (500 MHz, $CDCl_3$) δ 7.38 (s, 4H), 6.49 (s, 1H), 3.90 (s, 3H), 3.45 – 3.39 (m, 2H), 2.58 – 2.52 (m, 2H). ^{13}C NMR (125 MHz, $CDCl_3$) δ 170.27, 169.88, 162.91, 156.18, 141.50, 136.83, 132.05, 121.18, 116.89, 113.864, 106.87, 103.01, 52.74, 36.71, 28.71.HRMS (FAB) *m/z* [M+Na^+] for $C_{17}H_{15}BrClNO_5Na$: 449.9720; found, 449.9740.

methyl 3-chloro-4,6-dihydroxy-2-(3-((4-iodophenyl)amino)-3-oxopropyl)benzoate (28)—22 mg, 76% yield, white solid. ^{1}H NMR (500 MHz, $CDCl_3$ and CD_3OD) δ 7.55 (dd, 2H), 7.28 (dd, 2H), 6.43 (s, 1H), 3.89 (s, 3H), 3.41 – 3.39 (m, 2H), 2.56 – 2.53 (m, 2H). ^{13}C NMR (125 MHz, $CDCl_3$ and CD_3OD) δ 169.93, 162.88, 156.22, 149.99, 141.51, 137.99, 136.22, 129.72, 128.84, 126.65, 126.34, 121.46, 103.01, 52.74, 36.74, 28.69. HRMS (FAB) *m/z* [M + Na^+] for $C_{17}H_{15}ClINO_5Na$: 497.9683; found, 497.9656.

methyl 3-chloro-4,6-dihydroxy-2-(3-oxo-3-((4-(trifluoromethyl)phenyl)amino)propyl)benzoate (29)—31 mg, 74% yield, white amorphous solid: ^{1}H NMR (500 MHz, $(CD_3)_2CO$) δ 8.13 – 7.78 (m, 2H), 7.65 (dd, J = 8.8, 2.5 Hz, 2H), 6.51 (t, J = 1.7 Hz, 1H), 3.95 (t, J = 1.8 Hz, 3H), 3.44 (ddt, J = 10.2, 6.1, 1.8 Hz, 2H), 2.72 (ddt, J = 10.2, 6.3, 1.8 Hz, 2H); ^{13}C NMR (125 MHz, $(CD_3)_2CO$) δ (171.5, 171.4, 171.3, 162.2, 158.6, 142.9, 126.9, 126.9, 126.8, 126.8, 119.8, 119.8, 114.8, 108.2, 103.2, 52.9, 36.8, 28.8. HRMS (FAB) *m/z* [M + H^+] for $C_{18}H_{16}ClF_3NO_5$: 418.0669; found, 418.0669.

methyl 2-(3-([1,1'-biphenyl]-4-ylamino)-3-oxopropyl)-3-chloro-4,6-dihydroxybenzoate (30)—12.5 mg, 60% yield, white solid. ^{1}H NMR (400 MHz, $CDCl_3$) δ 7.57 – 7.48 (m, 6H), 7.41 – 7.23 (m, 3H), 7.15 (d, *J* = 5.6 Hz, 1H), 6.54 (s, 1H), 6.02 (s, 1H), 3.92 (s, 3H), 3.49 – 3.41 (m, 2H), 2.62 – 2.55 (m, 2H). ^{13}C NMR (125 MHz, $CDCl_3$) δ 170.41, 169.88, 162.96, 156.19, 141.64, 140.41, 137.25, 128.81, 127.70, 127.17, 126.84, 119.96, 113.88, 106.87, 102.96, 52.75, 36.75, 28.82. HRMS (FAB) *m/z* [M+Na^+] for $C_{23}H_{20}ClNO_5Na$: 448.0928; found, 448.0946.

methyl 3-chloro-4,6-dihydroxy-2-(3-oxo-3-(p-tolylamino)propyl)benzoate (31)—14 mg, 76% yield, white solid. ^{1}H NMR (500 MHz, CD_3OD) δ 7.32 (dd, *J* = 8.5, 2.0 Hz, 2H), 7.08 – 7.02 (m, 2H), 6.47 (s, 1H), 3.88 (s, 3H), 3.45 – 3.37 (m, 2H), 2.56 – 2.49 (m, 2H), 2.24 (s, 3H). ^{13}C NMR (125 MHz, CD_3OD) δ 168.00, 167.60, 167.51, 154.20, 139.34, 132.64, 131.47, 131.44, 127.00, 117.33, 117.21, 111.59, 104.03, 100.23, 50.14, 34.05, 26.29, 18.34.HRMS (FAB) *m/z* [M+Na^+] for $C_{18}H_{18}ClNO_5Na$: 386.0771; found, 386.1007.

methyl 3-chloro-4,6-dihydroxy-2-(3-((4-hydroxyphenyl)amino)-3-oxopropyl)benzoate (32)—8.8 mg, 48% yield, white solid. ^{1}H NMR (500 MHz, CD_3OD) δ 7.36 – 7.27 (m, 2H), 6.74 – 6.63 (m, 2H), 6.38 (s, 1H), 3.88 (s, 3H), 3.30–3.28 (m, 2H), 2.64 – 2.55 (m, 2H). ^{13}C NMR (125 MHz, CD_3OD) δ 172.98, 171.64, 161.37, 158.85, 155.34, 142.31, 131.72, 123.38, 116.18, 114.89, 109.69, 103.11, 52.84, 36.88, 29.19.HRMS (FAB) *m/z* [M+Na^+] for $C_{17}H_{16}ClNO_6Na$: 388.0564; found, 388.0556.

methyl 3-chloro-4,6-dihydroxy-2-(3-((4-methoxyphenyl)amino)-3-oxopropyl)benzoate (33)—32 mg, 73% yield, white powder. ^{1}H NMR (500 MHz, CD_3OD): δ 7.42–7.37 (m, 2 H), 6.84–6.79 (m, 2 H), 6.41 (s, 1 H), 3.90 (s, 3 H), 3.75 (s, 3 H), 3.45–3.39 (m, 2 H), 2.58–2.52 (m, 2 H). ^{13}C NMR (125 MHz, CD_3OD): δ 170.74, 170.72, 161.9, 157.8, 156.1, 142.0, 131.1, 121.6, 114.6, 114.0, 106.0, 102.3, 55.4, 52.4, 36.1, 28.6. HRMS (FAB) *m/z* [M+Na^+] for $C_{18}H_{18}ClNO_6Na$: 402.0720; found, 402.0725.

methyl 2-(3-((4-aminophenyl)amino)-3-oxopropyl)-3-chloro-4,6-dihydroxybenzoate (34)—8 mg, 33% yield, dark brown solid. ^{1}H NMR (400 MHz, CD_3OD) δ 7.45 – 7.27 (m, 2H), 6.90 – 6.74 (m, 2H), 6.50 (s, 1H), 4.00 (s, 3H), 3.41 (dt, *J* = 3.2, 1.7 Hz, 13H), 2.77 – 2.65 (m, 2H). ^{13}C NMR (125 MHz, $CDCl_3$ and CD_3OD) δ 170.59, 169.91, 162.49, 156.88, 143.10, 141.99, 129.23, 121.91, 115.51, 106.47, 102.65, 52.63, 49.80, 36.43, 29.70, 28.90. HRMS (FAB) *m/z* [M+Na^+] for $C_{17}H_{17}ClN_2O_5Na$: 387.0826; found, 387.0836.

methyl 3-chloro-2-(3-((4-cyanophenyl)amino)-3-oxopropyl)-4,6-dihydroxybenzoate (35)—13.6 mg, 72% yield, white solid. ^{1}H NMR (500 MHz, $CDCl_3$) δ 7.71 – 7.60 (m, 4H), 6.56 (s, 1H), 3.98 (s, 3H), 3.53 – 3.46 (m, 2H), 2.70 – 2.64 (m, 2H). ^{13}C NMR (125 MHz, $CDCl_3$) δ 170.97, 170.41, 162.19, 157.38, 142.28, 141.72, 133.26, 119.32, 118.94, 114.44, 106.70, 106.26, 102.66, 52.59, 36.46, 28.41.HRMS (FAB) *m/z* [M+H] for $C_{18}H_{15}ClN_2O_5$: 375.0748; found, 375.2276.

methyl 3-chloro-2-(3-((4-ethynylphenyl)amino)-3-oxopropyl)-4,6-dihydroxybenzoate (36)—18 mg, 95% yield, off-white solid. ^{1}H NMR (400 MHz,

$CDCl_3$): δ 7.51–7.46 (m, 2 H), 7.39–7.34 (m, 2 H), 6.38 (s, 1 H), 3.87 (s, 3 H), 3.48–3.32 (m, 5 H), 3.01 (s, 1 H), 2.60–2.53 (m, 2 H); ^{13}C NMR (125 MHz, $CDCl_3$ and CD_3OD): δ 171.2, 170.7, 161.8, 157.8, 141.9, 138.7, 132.7, 119.2, 117.1, 114.6, 106.0, 102.3, 83.3, 76.5, 52.3, 36.0, 28.3. HRMS (FAB) *m/z* [M+Na$^+$] for $C_{19}H_{16}ClNO_5Na$: 396.0615; found, 396.0608.

methyl 3-chloro-4,6-dihydroxy-2-(3-((4-isopropylphenyl)amino)-3-oxopropyl)benzoate (37)—26 mg, 87% yield, white solid. ^{1}H NMR (500 MHz, $(CD_3)_2CO$) δ 9.13 (s, 1H), 7.74 – 7.52 (m, 2H), 7.27 – 7.13 (m, 2H), 6.54 (t, *J* = 1.5 Hz, 1H), 4.08 – 3.89 (m, 3H), 3.54 – 3.36 (m, 2H), 2.90 (td, *J* = 7.0, 2.1 Hz, 1H), 2.69 (ddt, *J* = 8.1, 6.5, 1.6 Hz, 2H), 2.15 – 2.11 (m, 1H), 1.25 (dt, *J* = 6.9, 1.4 Hz, 7H). ^{13}C NMR (125 MHz, $(CD_3)_2CO$) δ 171.36, 170.68, 162.29, 158.56, 144.45, 143.28, 138.23, 138.15, 127.23, 120.07, 114.76, 108.22, 103.09, 52.91, 36.73, 34.28, 29.03, 24.41. HRMS (FAB) *m/z* [M +Na$^+$] for $C_{20}H_{22}ClNO_5Na$: 414.1187; found, 414.1165.

methyl 3-chloro-4,6-dihydroxy-2-(3-oxo-3-(pyridin-2-ylamino)propyl)benzoate (38)—^{1}H NMR (500 MHz, $(CD_3)_2CO$) δ 8.39 – 8.07 (m, 2H), 7.80 (dd, *J* = 8.7, 7.4, 1.8 Hz, 1H), 7.10 (dd, *J* = 7.3, 4.8, 1.1 Hz, 1H), 6.55 (s, 1H), 3.99 (s, 3H), 3.57 – 3.42 (m, 2H), 2.98 – 2.77 (m, 2H). ^{13}C NMR (125 MHz, $(CD_3)_2CO$) δ 171.60, 162.34, 158.67, 153.19, 148.85, 143.11, 138.72, 120.02, 114.86, 114.29, 108.11, 103.12, 52.92, 36.62, 28.77. HRMS (FAB) *m/z* [M+Na$^+$] for $C_{16}H_{15}ClN_2O_5Na$: 373.0669; found, 373.0630.

methyl 3-chloro-4,6-dihydroxy-2-(3-oxo-3-(pyridin-3-ylamino)propyl)benzoate (39)—23 mg, 65% yield, white amorphous solid: ^{1}H NMR (500 MHz, $(CD_3)_2CO$) δ 8.80 (dd, *J* = 4.7, 1.5 Hz, 1H), 8.35 (dd, *J* = 9.0, 1.5 Hz, 1H), 7.51 (dd, *J* = 9.0, 4.7 Hz, 1H), 6.40 (s, 1H), 3.82 (s, 3H), 3.48 – 3.21 (m, 2H), 2.80 – 2.75 (m, 2H); ^{13}C NMR(125 MHz, $(CD_3)_2CO$): δ 158.6, 145.2, 143.0, 141.9, 126.7, 124.2, 103.1, 52.9, 36.7, 36.6, 28.8; HRMS (FAB) *m/z* [M +H$^+$] for $C_{16}H_6ClN_2O_5$: 351.0748; found, 351.0755.

methyl 3-chloro-4,6-dihydroxy-2-(3-oxo-3-(pyridin-4-ylamino)propyl)benzoate (40)—10 mg, 51% yield, white solid. ^{1}H NMR (500 MHz, $(CD_3)_2CO$ and CD_3OD) δ 9.55 (s, 1H), 8.53 – 8.40 (m, 2H), 7.73 – 7.61 (m, 2H), 6.52 (s, 1H), 3.95 (s, 3H), 3.52 – 3.40 (m, 2H), 2.75 – 2.71 (m, 2H). ^{13}C NMR (125 MHz, $(CD_3)_2CO$) δ 172.20, 171.54, 165.56, 162.82, 151.33 (2C), 146.82, 142.44, 113.98 (2C), 103.33, 54.98, 52.68, 36.96, 28.73. HRMS (FAB) *m/z* [M+Na$^+$] for $C_{16}H_{15}ClN_2O_5Na$: 373.0669; found, 373.0695.

methyl 3-chloro-4,6-dihydroxy-2-(3-oxo-3-(pyrazin-2-ylamino)propyl)benzoate (41)—9 mg, 26% yield, white powder. ^{1}H NMR (400 MHz, $CDCl_3$ and CD_3OD): δ 11.22 (s, 1 H), 9.58 (s, 1 H), 8.38–8.35 (m, 1 H), 8.27–8.23 (m, 1 H), 8.02 (bs, 1 H), 6.58 (s, 1 H), 3.98 (s, 3 H), 3.55–3.48 (m, 2 H), 2.76–2.69 (m, 2 H); ^{13}C NMR (125 MHz, $CDCl_3$ and CD_3OD): δ 171.5, 170.6, 161.7, 158.0, 148.5, 142.2, 141.3, 139.3, 136.7, 114.6, 105.9, 102.3, 52.3, 35.7, 27.9. HRMS (FAB) *m/z* [M+Na$^+$] for $C_{15}H_{14}ClN_3O_5Na$: 374.0520; found, 374.0524.

methyl 3-chloro-4,6-dihydroxy-2-(3-oxo-3-(pyridazin-3-ylamino)propyl)benzoate (42)—26 mg, yield 74%, white amorphous solid: ^{1}H NMR

(500 MHz, $(CD_3)_2CO$) δ 10.04 (s, 1H), 8.92 (dd, *J* = 4.7, 1.5 Hz, 1H), 8.47 (dd, *J* = 9.0, 1.5 Hz, 1H), 7.63 (dd, *J* = 9.0, 4.7 Hz, 1H), 6.52 (s, 1H), 3.94 (s, 3H), 3.54 – 3.38 (m, 2H), 2.99 – 2.84 (m, 2H); ^{13}C NMR (125 MHz, $(CD_3)_2CO$) δ 158.78, 149.10, 142.85, 128.79, 118.60, 118.54, 103.20, 52.93, 36.60, 28.60; HRMS (FAB) *m/z* [M +Na^+] for $C_{15}H_{14}ClN_3O_5Na$: 374.0520; found, 374.0534.

methyl 3-chloro-4,6-dihydroxy-2-(3-oxo-3-(pyrimidin-5-ylamino)propyl)benzoate (43)—23 mg, 66% yield, white amorphous solid: ^1H NMR (400 MHz, $CDCl_3$-MeOD) δ 9.01 (s, 2H), 8.84 (s, 1H), 6.42 (s, 1H), 3.91 (s, 3H), 3.59 – 3.36 (m, 2H), 2.70 – 2.51 (m, 2H); ^{13}C NMR ($CDCl_3$, 125 MHz): δ 172.1, 170.9, 162.0, 158.1, 152.9, 147.6 (2), 141.8, 114.8 (2), 106.2, 102.6, 52.6, 35.7, 28.2; (FAB) *m/z* [M + H^+] for $C_{15}H_{15}ClN_3O_5$: 352.0712; found, 352.0712.

methyl 3-chloro-4,6-dihydroxy-2-(3-oxo-3-(pyrimidin-2-ylamino)propyl)benzoate (44)—21 mg, yield 60%, white amorphous solid: ^1H NMR (500 MHz, $(CD_3)_2CO$) δ 9.04 (d, *J* = 1.3 Hz, 2H), 8.83 (s, 1H), 6.51 (s, 1H), 3.94 (s, 3H), 3.57 – 3.31 (m, 2H), 2.82 – 2.69 (m, 2H); ^{13}C NMR(125 MHz, $(CD_3)_2CO$): δ 171.7, 171.2, 158.6, 154.2, 148.0, 147.9, 142.7, 135.6, 135.5, 114.8, 108.3, 103.2, 52.9, 36.4, 28.7; HRMS (FAB) *m/z* [M + Na^+] for $C_{15}H_{14}ClN_3O_5Na$: 374.0520; found, 374.0527.

methyl 2-(3-((1,2,4-triazin-5-yl)amino)-3-oxopropyl)-3-chloro-4,6-dihydroxybenzoate (45)—8.7 mg, 12% yield, yellow powder. ^1H NMR (500 MHz, $CDCl_3$ and CD_3OD): δ 8.89 (d, *J* = 2.5 Hz, 1 H), 8.47 (d, *J* = 2.5 Hz, 1 H), 6.37 (s, 1 H), 3.80 (s, 3 H), 3.45–3.38 (m, 2 H), 2.89–2.80 (m, 2 H). ^{13}C NMR (125 MHz, $CDCl_3$ and CD_3OD): δ 171.8, 170.7, 161.8, 158.8, 157.9, 149.7, 145.1, 141.5, 114.6, 105.9, 102.3, 52.3, 36.2, 27.6. HRMS (FAB) *m/z* [M+Na^+] for $C_{14}H_{13}ClN_4O_5Na$: 375.0472; found, 375.0468.

methyl 3-chloro-4,6-dihydroxy-2-(3-oxo-3-(thiazol-2-ylamino)propyl)benzoate (46)—30 mg, 84% yield, white amorphous solid: ^1H NMR (500 MHz, $(CD_3)_2CO$) δ 7.40 (d, *J* = 3.6 Hz, 1H), 7.11 (d, *J* = 3.6 Hz, 1H), 6.52 (s, 1H), 3.94 (s, 3H), 3.57 – 3.34 (m, 2H), 2.98 – 2.78 (m, 2H); ^{13}C NMR ($(CD_3)_2CO$, 125 MHz) δ 171.3, 170.7, 162.4, 158.9, 158.7 , 142.7, 138.5, 114.9, 113.9, 108.2, 103.3, 53.0, 35.4, 28.6. (FAB) *m/z* [M + H^+] calcd for $C_{14}H_{14}ClN_2O_5S$: 357.0312; found, 357.0323.

methyl 2-(3-((1,3,4-thiadiazol-2-yl)amino)-3-oxopropyl)-3-chloro-4,6-dihydroxybenzoate (47)—28 mg, 78% yield, white amorphous solid: ^1H NMR (500 MHz, $CDCl_3$-MeOD,) δ 8.79 (d, *J* = 0.9 Hz, 1H), 6.44 (d, *J* = 0.9 Hz, 1H), 3.89 (d, *J* = 0.9 Hz, 3H), 3.62 – 3.30 (m, 2H), 2.93 – 2.40 (m, 4H); ^{13}C NMR($CDCl_3$-MeOD, 125 MHz): 171.0, 170.9, 162.3, 159.5, 158.1, 148.0, 141.3, 114.9, 106.1, 102.8, 52.6, 34.9, 28.0. (FAB) *m/z* [M + Na^+] for $C_{13}H_{12}ClN_3O_5SNa$: 380.0084; found, 380.0090.

methyl 2-(3-((1,2,4-thiadiazol-5-yl)amino)-3-oxopropyl)-3-chloro-4,6-dihydroxybenzoate (48)—19 mg, 53% yield, white amorphous solid: ^1H NMR (400 MHz, $CDCl_3$-MeOD) δ 8.19 (s, 1H), 7.72 (s, 1H), 6.36 (s, 1H), 3.83 (s, 3H), 3.50 – 3.32 (m, 2H), 2.91 – 2.69 (m, 2H); ^{13}C NMR ($CDCl_3$-MeOD, 125 MHz): δ 179.3, 176.3, 174.5,

163.0, 162.2.161.6, 144.8, 118.6, 110.2, 106.4, 56.3, 38.1, 33.5. (FAB) *m/z* [M + Na^+] for $C_{13}H_{12}ClN_3O_5SNa$: 380.0084; found, 380.0078.

methyl 3-chloro-4,6-dihydroxy-2-(3-(methyl(phenyl)amino)-3-oxopropyl)benzoate (49)—28 mg, 77% yield, white amorphous solid: ^{1}H NMR (400 MHz, $CDCl_3$-MeOD) δ 7.34 (dd, *J* = 8.4, 6.8 Hz, 2H), 7.31 – 7.23 (m, 2H), 7.15 – 7.08 (m, 2H), 6.33 (s, 1H), 3.87 (s, 3H), 3.25 (d, *J* = 7.5 Hz, 5H), 2.35 – 2.27 (m, 2H); ^{13}C NMR ($CDCl_3$-CH_3OH, 125 MHz) δ 172.9, 171.0, 162.1, 157.9, 143.7, 142.3, 130.0 (2), 128.1, 127.2 (2), 114.8, 106.0, 102.3, 52.4, 37.6, 33.4, 28.9; (FAB) *m/z* [M + H^+]for $C_{18}H_{19}ClNO_5$: 364.0952; found, 364.0943.

methyl 3-chloro-2-(3-(ethyl(phenyl)amino)-3-oxopropyl)-4,6-dihydroxybenzoate (50)—30 mg, 79% yield, white amorphous solid: ^{1}H NMR (500 MHz, $CDCl_3$-MeOD) δ 7.34 (t, *J* = 7.7 Hz, 2H), 7.31 – 7.24 (m, 2H), 7.06 (dd, *J* = 7.3, 1.7 Hz, 2H), 6.33 (d, *J* = 4.0 Hz, 1H), 3.87 (d, *J* = 3.9 Hz, 3H), 3.70 (q, *J* = 7.1 Hz, 3H), 3.27 – 3.19 (m, 2H), 2.34 – 2.16 (m, 2H), 1.07 (td, *J* = 7.2, 3.4 Hz, 3H); ^{13}C NMR ($CDCl_3$-MeOD, 125 MHz) δ 172.3, 171.0, 162.0, 157.9, 142.3, 141.9, 129.9 (2), 128.3 (2), 128.2, 114.7, 106.1, 102.2, 52.4, 44.3, 33.7, 28.8, 13.0; (FAB) *m/z* [M + H^+] for $C_{19}H_{21}ClNO_5$: 378.1108; found, 378.1108.

methyl 3-chloro-4,6-dihydroxy-2-(3-(isopropyl(phenyl)amino)-3-oxopropyl)benzoate (51)—A solution of benzyl protected acid **1a** (100 mg, 0.22 mmol) in dry CH_2Cl_2 was treated with oxalyl chloride (23 μL, 0.33 mmol) under Ar atmosphere and then stirred at room temperature for 2 h. The solvent was then removed *in vacuo* and the residue was placed under high vacuum for 30 min to remove any unreacted oxalyl chloride. The residue was then redissolved in dry CH_2Cl_2 (3 mL), cooled to 0^{o}C, and was treated sequentially with diisopropylethyl amine (57 μL, 0.33 mmol) and *N*-isopropylaniline (72μL, 0.33 mmol). The resulting mixture was stirred at room temperature overnight under Ar. The solvent was removed *in vacuo* and the residue was passed through a short pad of silica (1:1, EtOAc:Hexanes) and was concentrated to afford the amide crude product, which was dissolved in MeOH (5 mL) and treated with Pd/C (10 mol%, 23 mg). The resulting suspension was charged with a hydrogen balloon and stirred under H_2 at room temperature. When debenzylation was found to be complete, the mixture was filtered through celite, concentrated, and purified on silica gel chromatography (1:1, EtOAc:Hexanes) to afford compound **51** (30 mg, 35% yield over 2 steps) as a white solid. ^{1}H NMR (400 MHz, $CDCl_3$): δ 7.45–7.27 (m, 13 H), 7.06–7.12 (m, 2 H), 6.41 (s, 1 H), 5.07 (hept, *J* = 6.8 Hz, 1 H), 5.04 (s, 2 H), 4.98 (s, 2 H), 3.88 (s, 3 H), 3.03–2.93 (m, 2 H), 2.30–2.21 (m, 2 H), 1.08 (d, *J* = 6.8 Hz, 6 H). ^{13}C NMR (125 MHz, $CDCl_3$): δ 171.1, 167.5, 155.4, 154.5, 138.6, 138.3, 136.2, 135.9, 130.3, 129.2, 128.6, 128.5, 128.1, 127.9, 126.9, 126.8, 118.4, 115.5, 98.2, 70.9, 70.8, 52.4, 45.8, 34.4, 27.9, 21.0. HRMS (FAB) *m/z* [M+Na^+] for $C_{20}H_{22}ClNO_5Na$: 414.1084; found, 414.1076.

methyl 3-chloro-4,6-dihydroxy-2-(3-(hydroxy(phenyl)amino)-3-oxopropyl)benzoate (52)—A round bottom flask was charged with aldehyde **1b** (100 mg, 0.2 mmol), nitrosobenzene (22 mg, 0.2 mmol), and 6,7-Dihydro-2-

pentafluorophenyl-5H–pyrrolo[2,1-c]-1,2,4-trazolium tetrafluoroborate (**catalyst**, 7 mg, 0.02 mmol) and purged with argon. The mixture was then dissolved in CH_2Cl_2 (1.5 mL) followed by addition of DBU (3μL, 0.02 mmol) and stirred at room termperature for 30 min. Upon completion, the solvent removed *in vacuo*. The resulting residue was dissolved in THF (2 mL) and treated with TBAF (0.5 mL of 1M solution). After complete silyl-deprotection, saturated aqueous NH_4Cl was added and extracted 3x with EtOAc (15 mL). The crude material was purified via flash chromatography (SiO_2, 2:3 EtOAc:Hexanes) to yield **52** as an off white solid (16 mg, 94%). ^{1}H NMR (400 MHz, $CDCl_3$): δ 11.30 (s, 1 H), 7.45–7.32 (m, 5 H), 6.52 (s, 1 H), 3.88 (s, 3 H), 3.42–3.36 (m, 2 H), 2.73–2.48 (m, 2 H). ^{13}C NMR (125 MHz, $CDCl_3$): δ 170.74, 163.10, 156.32 (2 C), 141.18, 137.80, 129.57, 126.54, 119.88, 114.00, 106.92, 103.03 (2 C), 52.71, 31.51, 28.84, 28.82. HRMS (FAB) *m/z* [M+Li^+] for $C_{17}H_{16}ClNO_6Li$: 372.0826, found 372.0823.

methyl 3-chloro-4,6-dihydroxy-2-(3-(indolin-1-yl)-3-oxopropyl)benzoate (53)— 15 mg, 25% yield, white solid. ^{1}H NMR (400 MHz, $CDCl_3$): δ ^{1}H NMR (400 MHz, $CDCl_3$ and CD_3OD) δ 8.19 (d, *J* = 8.0 Hz, 1H), 7.24 – 7.10 (m, 2H), 6.99 (d, *J* = 1.2 Hz, 1H), 6.42 (d, *J* = 1.5 Hz, 1H), 4.00 (dd, *J* = 9.1, 7.8 Hz, 2H), 3.88 (d, *J* = 2.8 Hz, 3H), 3.52 – 3.40 (m, 2H), 3.16 (t, *J* = 8.4 Hz, 2H), 2.75 – 2.60 (m, 2H). ^{13}C NMR (125 MHz, $CDCl_3$ and CD_3OD) δ 170.88, 170.71, 162.06, 157.89, 142.74, 142.21, 131.21, 127.50, 124.61, 123.81, 116.90, 114.64, 106.04, 102.42, 102.35, 52.51, 50.07, 49.72, 49.55, 49.38, 49.21, 49.03, 48.86, 48.69, 47.97, 35.08, 27.95, 27.84. HRMS (FAB) *m/z* [M+Na^+] for $C_{19}H_{18}ClNO_5Na$: 398.0771; found, 398.0773.

methyl 3-chloro-2-(3-((2,4-dibromophenyl)amino)-3-oxopropyl)-4,6-dihydroxybenzoate (54)—21 mg, 83%, white solid. ^{1}H NMR (500 MHz, $CDCl_3$ and CD_3OD) δ 8.22 (d, *J* = 8.9 Hz, 1H), 7.63 (dd, *J* = 2.2, 1.2 Hz, 1H), 7.49 – 7.33 (m, 1H), 6.44 (d, *J* = 1.0 Hz, 1H), 3.90 (d, *J* = 1.2 Hz, 3H), 3.47 – 3.39 (m, 2H), 2.72 – 2.54 (m, 2H). ^{13}C NMR (125 MHz, $CDCl_3$ and CD_3OD) δ 170.52, 162.40, 157.48, 141.32, 134.74, 134.42, 131.43, 122.78, 116.73, 114.47, 113.56, 106.14, 102.72, 52.64, 36.99, 28.77. HRMS (FAB) *m/z* [M+Na^+] for $C_{17}H_{14}Br_2ClNO_5Na$: 527.8927, found 527.8935.

methyl 3-chloro-2-(3-((3,5-dichlorophenyl)amino)-3-oxopropyl)-4,6-dihydroxybenzoate (55)—19 mg, 91% yield, white solid. ^{1}H NMR (400 MHz, $CDCl_3$): δ 11.07 (s, 1 H), 7.51 (d, *J* = 1.88 Hz, 2 H), 7.29 (s, 1 H), 7.11 (t, *J* = 1.7 Hz, 1 H), 6.60 (s, 1 H), 6.13 (s, 1 H), 3.98 (s, 1 H), 3.52–3.43 (m, 2 H), 2.75–2.49 (m, 2 H). ^{13}C NMR (125 MHz, $CDCl_3$ and CD_3OD): δ 170.73, 170.50, 162.48, 157.22, 141.80, 139.98, 135.30, 124.08, 117.85, 114.43, 106.49, 102.87, 52.77, 36.52, 28.62. HRMS (FAB) *m/z* [M+Na^+] for $C_{17}H_{14}Cl_3NO_5Na$: 439.9830, found 439.9840.

methyl 2-(3-((4-bromo-3-chlorophenyl)amino)-3-oxopropyl)-3-chloro-4,6-dihydroxybenzoate (56)—24 mg, 89% yield, white solid. ^{1}H NMR (500 MHz, $(CD_3)_2CO$) δ 8.12 (d, *J* = 2.5 Hz, 1H), 7.64 (d, *J* = 8.8 Hz, 1H), 7.48 (dd, *J* = 8.8, 2.5 Hz, 1H), 6.52 (s, 1H), 3.96 (s, 3H), 3.50 – 3.37 (m, 2H), 2.80 – 2.63 (m, 2H). ^{13}C NMR (125 MHz, $(CD_3)_2CO$) δ 170.45, 170.32, 161.23, 157.73, 141.96, 140.00, 133.72, 120.46, 119.04,

114.46, 113.91, 107.27, 102.20, 52.01, 35.87, 27.84. HRMS (FAB) *m/z* [M+Na^+] for $C_{17}H_{14}BrCl_2NO_5Na$: 483.9432; found, 398.9333.

methyl 2-(3-((2-bromo-3-chlorophenyl)amino)-3-oxopropyl)-3-chloro-4,6-dihydroxybenzoate (57)—23 mg, 72% yield, white amorphous solid: ^1H NMR (500 MHz, $CDCl_3$-MeOD) δ 8.14 (d, *J* = 7.9 Hz, 1H), 7.25 – 7.15 (m, 2H), 6.40 (d, *J* = 1.2 Hz, 1H), 3.90 (d, *J* = 1.2 Hz, 3H), 3.46 – 3.37 (m, 3H), 2.72 – 2.62 (m, 2H); ^{13}C NMR ($CDCl_3$-MeOD, 125 MHz): δ 170.9, 170.6, 162.0, 158.1, 141.3, 137.3, 134.8, 128.5 (2), 125.6, 120.2, 114.7, 105.9, 102.5, 52.5, 36.8, 28.7; (FAB) m/z [M + Na^+] for $C_{17}H_{14}BrCl_2NO_5Na$: 483.9330; found, 483.9327.

methyl 3-chloro-2-(3-((6-chloropyridin-2-yl)amino)-3-oxopropyl)-4,6-dihydroxybenzoate (58)—27 mg, 70% yield, white amorphous solid: ^1H NMR (500 MHz, $(CD_3)_2CO$) δ 10.88 (1H, br s), 9.48 (1H, br s)8.09 (dd, *J* = 8.2, 1.8 Hz, 1H), 7.80 – 7.58 (m, 1H), 7.00 (dd, *J* = 7.9, 1.7 Hz, 1H), 6.63 – 6.10 (m, 1H), 3.93 (s, 3H), 3.46 – 3.10 (m, 2H), 2.91 – 2.55 (m, 2H); ^{13}C NMR (125 MHz, $(CD_3)_2CO$) δ 172.1, 171.5, 158.8, 153.3, 149.6, 143.1, 142.2, 119.9 (2), 115.0, 112.8, 108.3, 103.3, 53.1, 36.7, 28.8; (FAB) *m/z* [M + Na^+] for $C_{16}H_{14}Cl_2N_2O_5Na$: 407.0174; found, 407.0177.

methyl 2-(3-((5-bromopyridin-2-yl)amino)-3-oxopropyl)-3-chloro-4,6-dihydroxybenzoate (59)—29 mg, 68% yield, white amorphous solid: ^1H NMR (500 MHz, $CDCl_3$-MeOD) δ 8.31 – 8.19 (m, 1H), 8.19 – 8.05 (m, 1H), 7.84 – 7.71 (m, 1H), 6.54 – 6.28 (m, 1H), 3.94 (s, 3H), 3.42 – 3.35 (m, 2H), 2.63 (dq, *J* = 12.7, 3.8, 2.1 Hz, 2H); ^{13}C NMR ($CDCl_3$-MeOD, 125 MHz): δ 171.5, 170.9, 162.1, 158.2, 150.2, 148.6, 141.6, 141.0, 115.5, 114.8, 114.5, 106.1, 102.6, 52.6, 36.4, 28.3. (FAB) *m/z* [M + Na^+] for $C_{16}H_{14}BrClN_2O_5Na$: 450.9672; found, 450.9681.

methyl 3-chloro-2-(3-((4-chloropyridin-2-yl)amino)-3-oxopropyl)-4,6-dihydroxybenzoate (60)—16 mg, 64% yield, white solid. ^1H NMR (500 MHz, $(CD_3)_2CO$) δ 8.41 (dd, *J* = 2.0, 0.6 Hz, 1H), 8.28 (dd, *J* = 5.3, 0.6 Hz, 1H), 7.19 (dd, *J* = 5.3, 1.9 Hz, 1H), 6.55 (s, 1H), 3.99 (s, 3H), 3.56 – 3.42 (m, 2H), 2.98 – 2.81 (m, 2H). ^{13}C NMR (125 MHz, $(CD_3)_2CO$) δ 172.16, 171.34, 162.41, 158.69, 154.30, 150.12, 145.43, 142.93, 120.15, 113.98, 108.12, 103.20, 52.93, 36.62, 28.62. HRMS (FAB) *m/z* [M+Na^+] for $C_{16}H_{14}Cl_2N_2O_5Na$: 407.0280; found, 407.0766.

methyl 3-chloro-2-(3-((3-chloropyridin-2-yl)amino)-3-oxopropyl)-4,6-dihydroxybenzoate (61)—21 mg, 55% yield, white amorphous solid: ^1H NMR (500 MHz, $(CD_3)_2CO$) δ 8.36 (dd, *J* = 4.7, 1.6 Hz, 1H), 7.92 (dd, *J* = 8.0, 1.6 Hz, 1H), 7.27 (ddd, *J* = 8.0, 4.7, 0.6 Hz, 1H), 6.52 (s, 1H), 3.97 (s, 3H), 3.55 – 3.39 (m, 2H), 3.00 – 2.76 (m, 2H). ^{13}C NMR (125 MHz, $(CD_3)_2CO$) δ 171.4, 171.28, 158.6, 149.3, 147.5, 143.2 (2), 139.3, 122.9 (2), 114.8, 108.14, 103.1, 52.9, 35.9, 28.8; (FAB) *m/z* [M + Na^+] for $C_{16}H_{14}Cl_2N_2O_5Na$: 407.0174; found 407.0174.

methyl 2-(3-((3-bromopyridin-2-yl)amino)-3-oxopropyl)-3-chloro-4,6-dihydroxybenzoate (62)—31 mg, 71% yield, white amorphous solid: ^1H NMR (400 MHz, $CDCl_3$-MeOD) δ 8.47 (dd, *J* = 4.7, 1.6 Hz, 1H), 7.98 (dd, *J* = 8.0, 1.6 Hz, 1H), 7.27 –

7.22(m, 1H), 6.34 (s, 1H), 3.85 (s, 3H), 3.35 – 3.29 (m, 2H), 2.91 – 2.65 (m, 2H). ^{13}C NMR (125 MHz, $CDCl_3$,): δ 172.8, 170.0, 161.2, 156.9, 149.7, 147.8, 141.7, 140.6, 124.9, 120.3, 113.8, 105.0, 101.4, 51.6, 36.3, 26.6. (FAB) *m/z* [M + Na^+] for $C_{16}H_{14}BrClN_2O_5Na$: 450.9672; found, 450.9677.

methyl 3-chloro-2-(3-((5-chlorothiazol-2-yl)amino)-3-oxopropyl)-4,6-dihydroxybenzoate (63)—17 mg, 44.7% yield, pale yellow amorphous solid: ^{1}H NMR (400 MHz, $(CD_3)_2CO$) δ 7.34 (s, 1H), 6.52 (s, 1H), 5.63 (s, 1H), 3.94 (s, 3H), 3.55 – 3.31 (m, 2H), 2.93 – 2.71 (m, 2H). ^{13}C NMR (125 MHz, $CDCl_3$-MeOD): δ 170.8 (2), 162.0, 158.1, 147.8, 141.8, 136.9, 129.5, 126.6, 125.3, 124.6, 120.9, 114.8, 106.2, 52.5, 30.8, 26.2; . HRMS (FAB) *m/z* [M +H^+] for $C_{14}H_{13}Cl_2N_2O_5S$: 390.9922; found, 390.9913.

methyl 2-(3-((5-bromothiazol-2-yl)amino)-3-oxopropyl)-3-chloro-4,6-dihydroxybenzoate (64)—36 mg, 83% yield, gray amorphous solid: ^{1}H NMR (500 MHz, $(CD_3)_2CO$) δ 7.33 (s, 1H), 6.52 (s, 1H), 3.94 (s, 2H), 3.60 – 3.28 (m, 2H), 2.93 – 2.78 (m, 2H). ^{13}C NMR(125 MHz, $(CD_3)_2CO$): δ 170.9, 170.9, 162.2, 159.6, 158.1, 141.4, 137.7, 114.9, 106.1, 102.7 (2), 52.7, 34.7, 28.1; HRMS (FAB) *m/z* [M +Na^+] for $C_{14}H_{12}BrClN_2O_5SNa$: 456.9237; found, 456.9238.

methyl 2-(3-((5-bromo-1,3,4-thiadiazol-2-yl)amino)-3-oxopropyl)-3-chloro-4,6-dihydroxybenzoate (65)—12 mg, 28% yield, gray amorphous solid: ^{1}H NMR (500 MHz, $(CD_3)_2CO$) δ 6.53 (s, 1H), 3.94 (s, 4H), 3.59 – 3.43 (m, 2H), 3.05 – 2.84 (m, 2H). ^{13}C NMR (125 MHz, $(CD_3)_2CO$): δ 171.7, 161.6, 158.7, 142.2, 134.8, 130.6, 114.9, 108.1, 103.3, 79.3, 53.0, 35.2, 21.1. HRMS (FAB) *m/z* [M +H^+] for $C_{13}H_{12}BrClN_3O_5S$: 435.9370; found, 435.9377.

Supplementary Material

Refer to Web version on PubMed Central for supplementary material.

Acknowledgments

The authors gratefully acknowledge the support of this project by NIH (CA109265).

References

1. Hartl FU. Molecular chaperones in cellular protein folding. Nature. 1996; 381:571–579. [PubMed: 8637592]
2. Hartl FU. Molecular chaperones in protein folding and proteostasis. Nature. 2011; 475:324–332. [PubMed: 21776078]
3. Pearl LH, Prodromou C. Structure and in vivo function of Hsp90. Curr. Opin. Struct. Biol. 2000; 10:46–51. [PubMed: 10679459]
4. Prodromou C, Pearl LH. Structure and functional relationships of Hsp90. Curr. Cancer Drug Targets. 2003; 3:301–323. [PubMed: 14529383]
5. Pearl LH, Prodromou C. Structure, function, and mechanism of the Hsp90 molecular chaperone. Adv. Protein Chem. 2001; 59:157–186. [PubMed: 11868271]
6. Meyer P, Prodromou C, Hu B, Vaughan C, Roe SM, Panaretou B, Piper PW, Pearl LH. Structural and functional analysis of the middle segment of Hsp90: implications for ATP hydrolysis and client protein and cochaperone interactions. Mol. Cell. 2003; 11:647–658. [PubMed: 12667448]

7. Panaretou B, Siligardi G, Meyer P, Maloney A, Sullivan JK, Singh S, Millson SH, Clarke PA, Naaby-Hansen S, Stein R, Cramer R, Mollapour M, Workman P, Piper PW, Pearl LH, Prodromou C. Activation of the ATPase activity of Hsp90 by the stress-regulated cochaperone aha1. Mol. Cell. 2002; 10:1307–1318. [PubMed: 12504007]
8. Marcu MG, Chadli A, Bouhouche I, Catelli M, Neckers LM. The heat shock protein 90 antagonist novobiocin interacts with a previously unrecognized ATP-binding domain in the carboxyl terminus of the chaperone. J. Biol. Chem. 2000; 275:37181–37186. [PubMed: 10945979]
9. Soti C, Racz A, Csermely P. A nucleotide-dependent molecular switch controls ATP binding at the C-terminal domain of Hsp90, N-terminal nucleotide binding unmasks a C-terminal binding pocket. J. Biol. Chem. 2002; 277:7066–7075. [PubMed: 11751878]
10. Whitesell L, Bagatell R, Falsey R. The stress response: implications for the clinical development of Hsp90 inhibitors. Curr. Cancer Drug Targets. 2003; 3:349–358. [PubMed: 14529386]
11. Whitesell L, Lindquist SL. Hsp90 and the chaperoning of cancer. Nat. Rev. Cancer. 2005; 5:761–772. [PubMed: 16175177]
12. Zhang H, Burrows F. Targeting multiple signal transduction pathways through inhibition of Hsp90. J. Mol. Med. 2004; 82:488–499. [PubMed: 15168026]
13. Kim YS, Alarcon SV, Lee S, Lee MJ, Giaccone G, Neckers L, Trepel JB. Update on Hsp90 inhibitors in clinical trial. Curr. Top. Med. Chem. 2009; 9:1479–1492. [PubMed: 19860730]
14. Biamonte MA, Van de Water R, Arndt JW, Scannevin RH, Perret D, Lee W. Heat shock protein 90: inhibitors in clinical trials. J. Med. Chem. 2010; 53:3–17. [PubMed: 20055425]
15. Holzbeierlein J, Windsperger A, Vielhauer G. Hsp90: a drug target? Curr. Oncol. Rep. 2010; 12:95–101. [PubMed: 20425593]
16. Sreedhar AS, Kalmar E, Csermely P, Shen YF. Hsp90 isoforms: functions, expression and clinical importance. FEBS Lett. 2004; 562:11–15. [PubMed: 15069952]
17. Peterson LB, Esker JD, Vielhauer GA, Blagg BS. The hERG channel is dependent upon the Hsp90α isoform for maturation and trafficking. Mol. Pharm. 2012; 9:1841–1846. [PubMed: 22554505]
18. McLaughlin M, Vandenbroeck K. The endoplasmic reticulum protein folding factory and its chaperones: new targets for drug discovery? Br. J. Pharmacol. 2011; 162:328–345. [PubMed: 20942857]
19. Goodman SL, Picard M. Integrins as therapeutic targets. Trends Pharmacol. Sci. 2012; 33:405–412. [PubMed: 22633092]
20. Dejeans N, Glorieux C, Guenin S, Beck R, Sid B, Rousseau R, Bisig B, Delvenne P, Buc Calderon P, Verrax J. Overexpression of Grp94 in breast cancer cells resistant to oxidative stress promotes high levels of cancer cell proliferation and migration: implications for tumor recurrence. Free Radic. Biol. Med. 2012; 52:993–1002. [PubMed: 22245095]
21. Suntharalingam A, Abisambra JF, O'Leary JC III, Koren J III, Zhang B, Joe MK, Blair LJ, Hill SE, Jinwal UK, Cockman M, Duerfeldt AS, Tomarev S, Blagg BS, Lieberman RL, Dickey CA. Glucose-regulated protein 94 triage of mutant myocilin through endoplasmic reticulum-associated degradation subverts a more efficient autophagic clearance mechanism. J. Biol. Chem. 2012; 287:40661–40669. [PubMed: 23035116]
22. Gullo CA, Teoh G. Heat shock protein: to present or not, that is the question. Immunol. Lett. 2004; 94:1–10. [PubMed: 15234529]
23. Obeng EA, Carlson LM, Gutman DM, Harrington WJ, Lee KP, Boise LH. Proteasome inhibitors induce a terminal unfolded protein response in myltiple myeloma cells. Blood. 2006; 107:4907–4916. [PubMed: 16507771]
24. Davenport EL, Moore HE, Dunlop AS, Sharp SY, Workman P, Morgan GJ, Davies FE. Heat shock protein inhibition is associated with activation of the unfolded protein response pathway in myeloma plasma cells. Blood. 2007; 110:2641–2649. [PubMed: 17525289]
25. Hua Y, White-Gilbertson S, Kellner J, Rachidi S, Usmani SZ, Chiosis G, DePinho R, Li Z, Liu B. Molecular chaperone gp96 is a novel therapeutic target for multiple myeloma. Clin. Cancer Res. 2013; 19:6242–6251. [PubMed: 24077352]

26. Duerfeldt AS, Peterson LB, Maynard JC, Ng CL, Eletto D, Ostrovsky O, Shinogle HE, Moore DS, Argon Y, Nicchitta CV, Blagg BSJ. Development of a Grp94 inhibitor. JACS. 2012; 134:9796–9804.
27. Rosser MF, Nicchitta CV. Ligand interactions in the adenosine nucleotide-binding domain of the Hsp90 chaperone, Grp94. I. Evidence for allosteric regulation of ligand binding. J. Biol. Chem. 2000; 275:22798–22805. [PubMed: 10816561]
28. Patel PD, Yan P, Seidler PM, Patel HJ, Sun W, Yang C, Que NS, Taldone T, Finotti P, Stephani RA, Gewirth DT, Chiosis G. Paralog-selective Hsp90 inhibitors define tumor-specific regulation of HER2. Nat. Chem. Biol. 2013; 9:677–684. [PubMed: 23995768]
29. Soldano KL, Jivan A, Nicchitta CV, Gewirth DT. Structure of the N-terminal domain of Grp94. Basis for ligand specificity and regulation. J. Biol. Chem. 2003; 278:48330–48338. [PubMed: 12970348]
30. Immormino RM, Metzger LE, Reardon PN, Dollins DE, Blagg BS, Gewirth DT. Different poses for ligand and chaperone in inhibitor-bound Hsp90 and Grp94: implications for paralog-specific drug design. J. Mol. Biol. 2009; 388:1033–1042. [PubMed: 19361515]
31. Clevenger RC, Blagg BSJ. Design, synthesis, and evaluation of a radicicol and geldanamycin chimera, radamide. Org. Lett. 2004; 6:4459–4462. [PubMed: 15548050]
32. Kim J, Felts S, Llauger L, He H, Huezo H, Rosen N, Chiosis G. Development of a fluorescence polarization assay for the molecular chaperone Hsp90. J. Biomol. Screen. 2004; 9:375–381. [PubMed: 15296636]
33. Taldone T, Patel PD, Patel M, Patel HJ, Evans CE, Rodina A, Ochiana S, Shah SK, Uddin M, Gewirth D, Chiosis G. Experimental and structural testing module to analyze paralogue-specificity and affinity in the Hsp90 inhibitors series. J. Med. Chem. 2013; 56:6803–6818. [PubMed: 23965125]
34. Hunter L. The C-F bond as a conformational tool in organic and biological chemistry. Beilstein J. Org. Chem. 2010:6. [PubMed: 20485588]
35. Wong FT, Patra PK, Seayad J, Zhang Y, Ying JY. N-heterocyclic carbine (NHC)-catalyzed direct amidation of aldehydes with nitroso compounds. Org. Lett. 2008; 10:2333–2336. [PubMed: 18476704]
36. Melnick J, Dul JL, Argon Y. Sequential interaction of the chaperones BiP and GRP94 with immunoglobulin chains in the endoplasmic reticulum. Nature. 1994; 370:373–375. [PubMed: 7913987]
37. Hadden KM, Blagg BSJ. Synthesis and evaluation of radamide analogues, a chimera of radicicol and geldanamycin. J. Org. Chem. 2009; 74:4697–4704. [PubMed: 19492825]
38. Duerfeldt AS, Brandt GEL, Blagg BSJ. Design, synthesis and biological evaluation of conformationally constrained cis-amide Hsp90 inhibitors. Org. Lett. 2009; 11:2353–2356. [PubMed: 19435295]
39. Shen G, Wang M, Welch TR, Blagg BSJ. Design, synthesis and structure activity relationships for chimeric inhibitors of Hsp90. J. Org. Chem. 2006; 71:7618–7631. [PubMed: 16995666]
40. Shen G, Blagg BSJ. Radester, a novel inhibitor of the Hsp90 protein folding machinery. Org. Lett. 2005; 7:2157–2160. [PubMed: 15901158]
41. Grad I, Cederroth CR, Walicki J, Grey C, Barluenga S, Winssinger N, De Massy B, Nef S, Picard D. The molecular chaperone Hsp90α is required for meiotic progression of spermatocytes beyond pachytene in the mouse. PLoS One. 2010; 5:e15770. [PubMed: 21209834]
42. Yu XM, Shen G, Neckers L, Blake H, Holzbeierlein J, Cronk B, Blagg BSJ. Hsp90 inhibitors identified from a library of novobiocin analogues. JACS. 2005; 127:12778–12779.
43. Burlison JA, Blagg BSJ. Synthesis and evaluation of coumermycin A1 analogues that inhibit the Hsp90 protein folding machinery. Org. Lett. 2006; 8:4855–4858. [PubMed: 17020320]
44. Burlison JA, Neckers L, Smith AB, Maxwell A, Blagg BSJ. Novobiocin: redesigning a DNA gyrase inhibitor for selective inhibition of Hsp90. JACS. 2006; 128:15529–15536.
44. Burlison JA, Avila C, Vielhauer G, Lubbers DJ, Holzbeierlein J, Blagg BSJ. Development of novobiocin analogues that manifest anti-proliferative activity against several cancer cell lines. J. Org. Chem. 2008; 73:2130–2137. [PubMed: 18293999]

45. Donnelly AC, Mays JR, Burlison JA, Nelson JT, Vielhauer G, Holzbeierlein J, Blagg BSJ. The design, synthesis, and evaluation of coumarin ring derivatives of the novobiocin scaffold that exhibit antiproliferative activity. J. Org. Chem. 2008; 73:8901–8920. [PubMed: 18939877]

46. Zhao H, Kusuma BR, Blagg BSJ. Synthesis and evaluation of noviose replacements on novobiocin that manifest antiproliferative activity. ACS Med. Chem. Lett. 2010; 1:311–315. [PubMed: 21904660]

47. Matts RL, Dixit A, Peterson LB, Sun L, Voruganti S, Kalyanaraman P, Hartson SD, Verkhivker GM, Blagg BSJ. Elucidation of the Hsp90 C-terminal binding site. ACS Chem. Biol. 2011; 6:800–807. [PubMed: 21548602]

48. Zhao H, Donnelly AC, Kusuma BR, Brandt GEL, Brown D, Rajewski RA, Vielhauer G, Holzbeierlein J, Cohen MS, Blagg BSJ. Engineering an antibiotic to fight cancer: Optimization of the novobiocin scaffold to produce anti-proliferative agents. J. Med. Chem. 2011; 54:3839–3853. [PubMed: 21553822]

49. Kusuma BR, Zhang L, Sundstrom T, Peterson LB, Dobrowsky RT, Blagg BSJ. Synthesis and evaluation of novologues as C-terminal Hsp90 inhibitors with cytoprotective activity against sensory neuron glucotoxicity. J. Med. Chem. 2012; 55:5797–5812. [PubMed: 22702513]

50. Khandelwal A, Hall JA, Blagg BSJ. Synthesis and structure-activity relationships of EGCG analogues, a recently identified Hsp90 inhibitor. J. Org. Chem. 2013; 78:7859–7884. [PubMed: 23834230]

51. Ostrovsky O, Ahmed NT, Argon Y. The chaperone activity of GRP94 toward insulin-like growth factor is necessary for the stress response to serum deprivation. Mol. Biol. Cell. 2009; 20:1855–1864. [PubMed: 19158397]

52. Wang JS, Wang FB, Zhang QG, Shen ZZ, Shao ZM. Enhanced expression of Rab27A gene by breast cancer cells promoting invasiveness and the metastasis potential by secretion of insulin-like growth factor-II. Mol. Cancer Res. 2008; 6:372–382. [PubMed: 18337447]

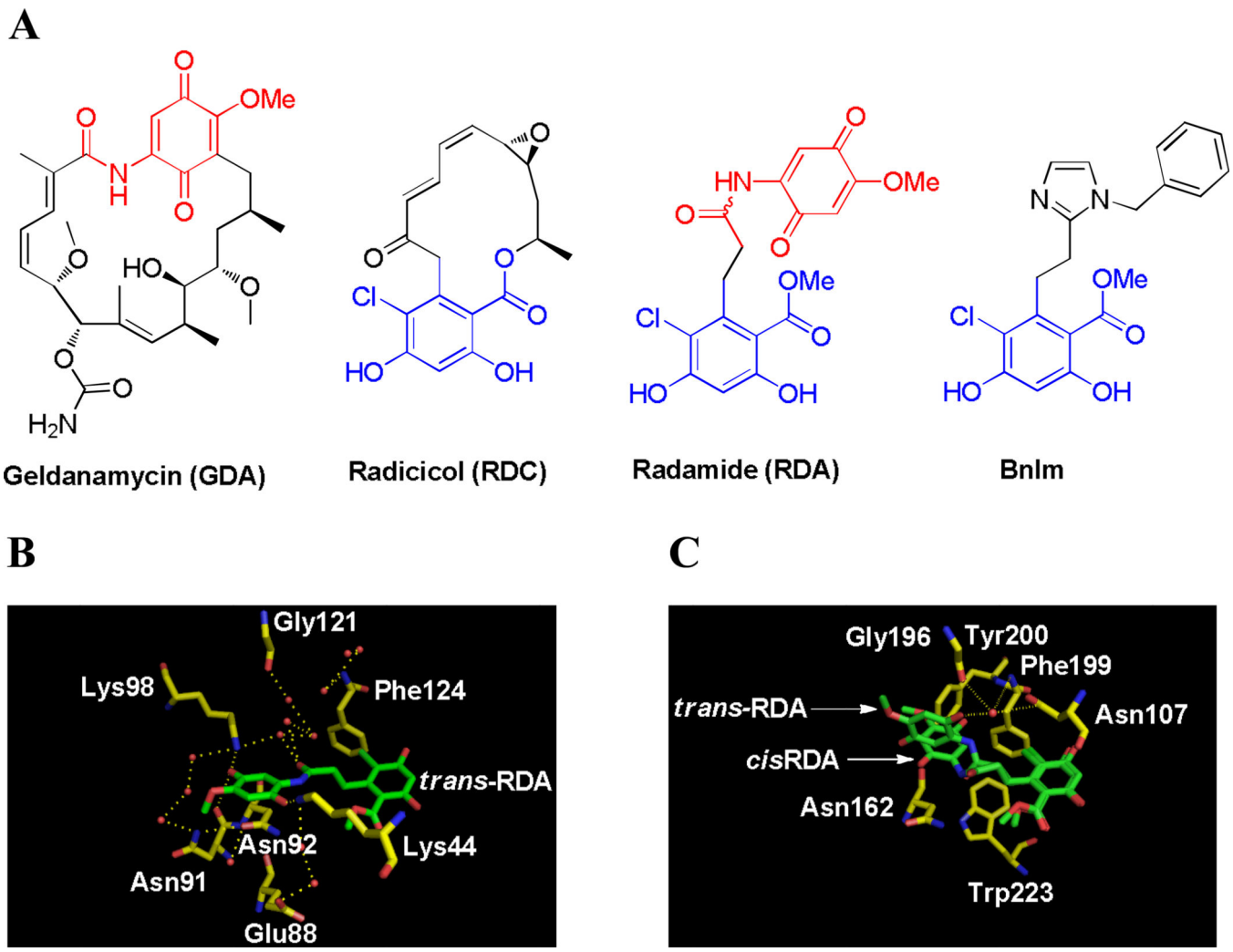

Figure 1.

(A) Structures of natural product Hsp90 inhibitors GDA and RDC, chimeric inhibitor RDA, and Grp94-selective inhibitor BnIm; (B) Co-crystal structure of RDA bound to Hsp90 (PDB: 2FXS); (C) Co-crystal structure of RDA bound to Grp94 (PDB: 2GFD)

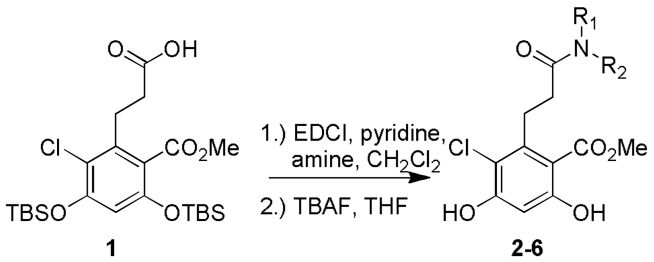

entry	R_1	R_2	% Tracer Bound
2	Ph	H	19.8 (±1.2)
3	CH_2Ph	H	65.8 (±3.5)
4	CH_2CH_2Ph	H	33.0 (±2.1)
5	NHNHPh	H	26.3 (±1.5)
6	cyclohexyl	H	26.1 (±1.4)

Figure 2.

Optimization of Amide Linker and Hydrophobic Moiety.a–d

[a] Compounds **2–6** (25 μM) were incubated with cGrp94 and FITC-GDA (tracer) for 24 h before fluorescence polarization values were determined. [b] DMSO (1%) served as a negative control (vehicle), and GDA (50 nM) served as the positive control. [c] All compounds tested at 25 μM. [d] All compounds were tested in triplicate.

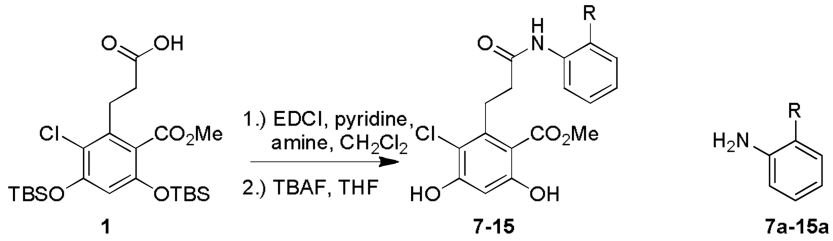

1 7-15 7a-15a

entry	R	% Tracer Bound
7	F	16.3 (±0.1)
8	Cl	0.1 (±0.1)
9	Br	6.1 (±0.1)
10	I	7.9 (±0.1)
11	CF_3	13.4 (±0.5)
12	OH	18.0 (±0.3)
13	OMe	16.1 (±0.6)
14	NH_2	20.5 (±1.0)
15	CH_3	3.4 (±0.1)

Figure 3.

Evaluation of 2-Phenyl Substitutions a–d

[a] Compounds **7–15** (25 μM) were incubated with cGrp94 and FITC-GDA (tracer) for 24 h before fluorescence polarization values were determined. [b] DMSO (1%) served as a negative control (vehicle), and GDA (50 nM) served as the positive control. [c] All compounds tested at 25 μM. [d] All compounds were tested in triplicate.

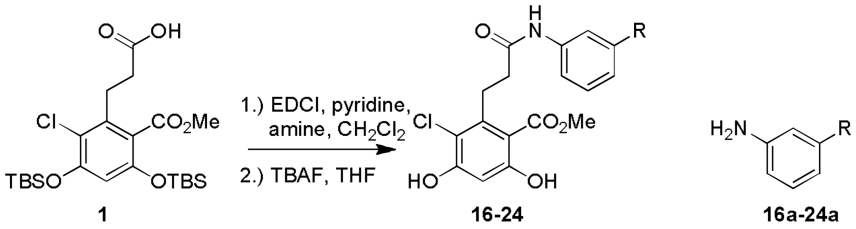

entry	R	% Tracer Bound
16	F	11.0 (±0.1)
17	Cl	0.1 (±0.1)
18	Br	9.3 (±0.3)
19	CF_3	39.4 (±3.0)
20	Ph	46.8 (±4.6)
21	OH	3.5 (±0.1)
22	OMe	27.4 (±0.9)
23	NH_2	17.4 (±0.8)
24	NHAc	8.3 (±0.1)

Figure 4.

Evaluation of 3-Phenyl Substitutionsa–d

[a] Compounds **16–24** (25 μM) were incubated with cGrp94 and FITC-GDA (tracer) for 24 h before fluorescence polarization values were determined. [b] DMSO (1%) served as a negative control (vehicle), and GDA (50 nM) served as the positive control. [c] All compounds tested at 25 μM. [d] All compounds were tested in triplicate.

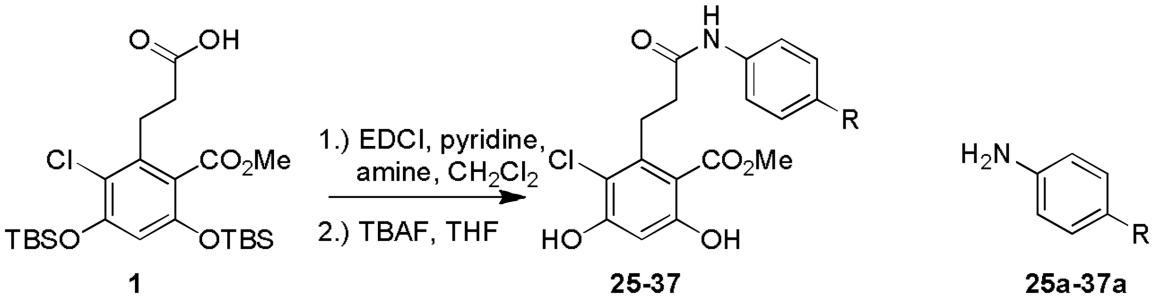

1 25-37 25a-37a

entry	R	% Tracer Bound
25	F	10.9 (±0.5)
26	Cl	15.7 (±0.3)
27	Br	2.1 (±0.1)
28	I	29.8 (±1.7)
29	CF_3	34.5 (±3.3)
30	Ph	85.0 (±16.4)
31	CH_3	18.7 (±0.7)
32	OH	6.5 (±0.2)
33	OMe	19.8 (±1.3)
34	NH_2	15.7 (±0.5)
35	CN	5.4 (±0.1)
36	CCH	12.7 (±1.1)
37	$CH(CH_3)_2$	59.0 (±3.2)

Figure 5.

Evaluation of 4-Phenyl Substitutionsa–d

[a] Compounds **25–37** (25 μM) were incubated with cGrp94 and FITC-GDA (tracer) for 24 h before fluorescence polarization values were determined. [b] DMSO (1%) served as a negative control (vehicle), and GDA (50 nM) served as the positive control. [c] All compounds tested at 25 μM. [d] All compounds were tested in triplicate.

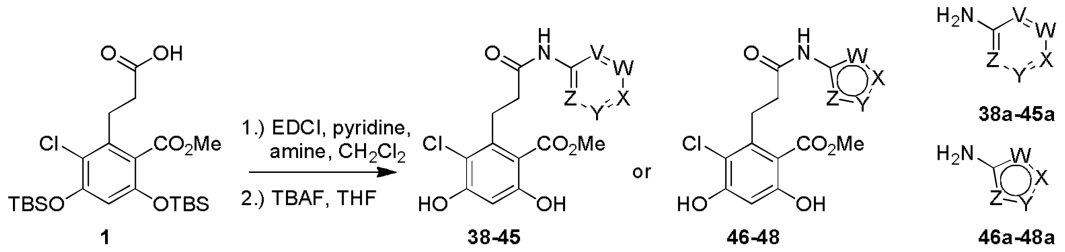

entry	V	W	X	Y	Z	%Tracer Bound
38	N	CH	CH	CH	CH	1.0 (±0.1)
39	CH	N	CH	CH	CH	14.9 (±1.0)
40	CH	CH	N	CH	CH	34.9 (±2.3)
41	N	CH	CH	N	CH	16.6 (±0.7)
42	N	N	CH	CH	CH	12.2 (±1.0)
43	CH	N	CH	N	CH	11.6 (±0.7)
44	N	CH	CH	CH	N	16.7 (±1.2)
45	N	CH	CH	N	N	19.5 (±1.2)
46		N	CH	CH	S	6.6 (±0.2)
47		N	N	CH	S	8.7 (±0.6)
48		N	CH	N	S	10.2 (±0.6)

Figure 6.

Evaluation of Heterocyclic Amidesa–d

[a] Compounds **38–48** (25 μM) were incubated with cGrp94 and FITC-GDA (tracer) for 24 h before fluorescence polarization values were determined. [b] DMSO (1%) served as a negative control (vehicle), and GDA (50 nM) served as the positive control. [c] All compounds tested at 25 μM. [d] All compounds were tested in triplicate.

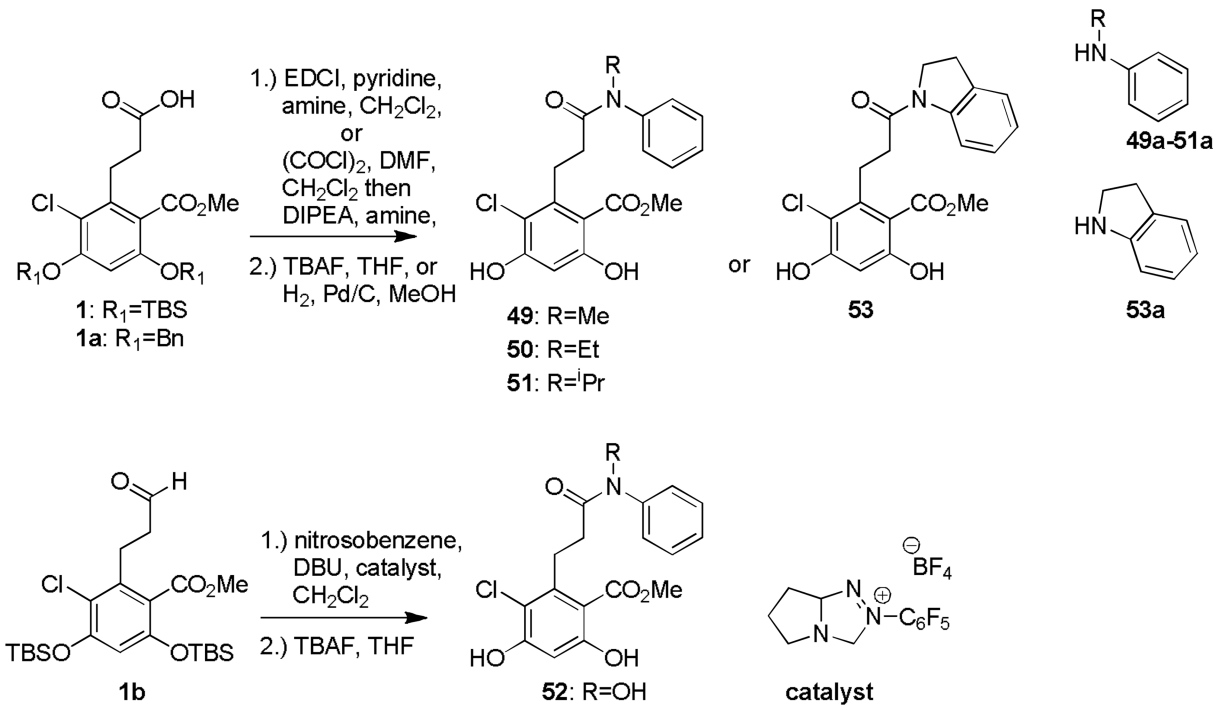

entry	% Tracer Bound
49	16.7 (±2.1)
50	18.6 (±2.8)
51	30.2 (±3.2)
52	2.5 (±0.8)
53	23.0 (±4.4)

Figure 7.

Evaluation of Amides **49–53**a–d

[a] Compounds **49–53** (25 μM) were incubated with cGrp94 and FITC-GDA (tracer) for 24 h before fluorescence polarization values were determined. [b] DMSO (1%) served as a negative control (vehicle), and GDA (50 nM) served as the positive control. [c] All compounds tested at 25 μM. [d] All compounds were tested in triplicate.

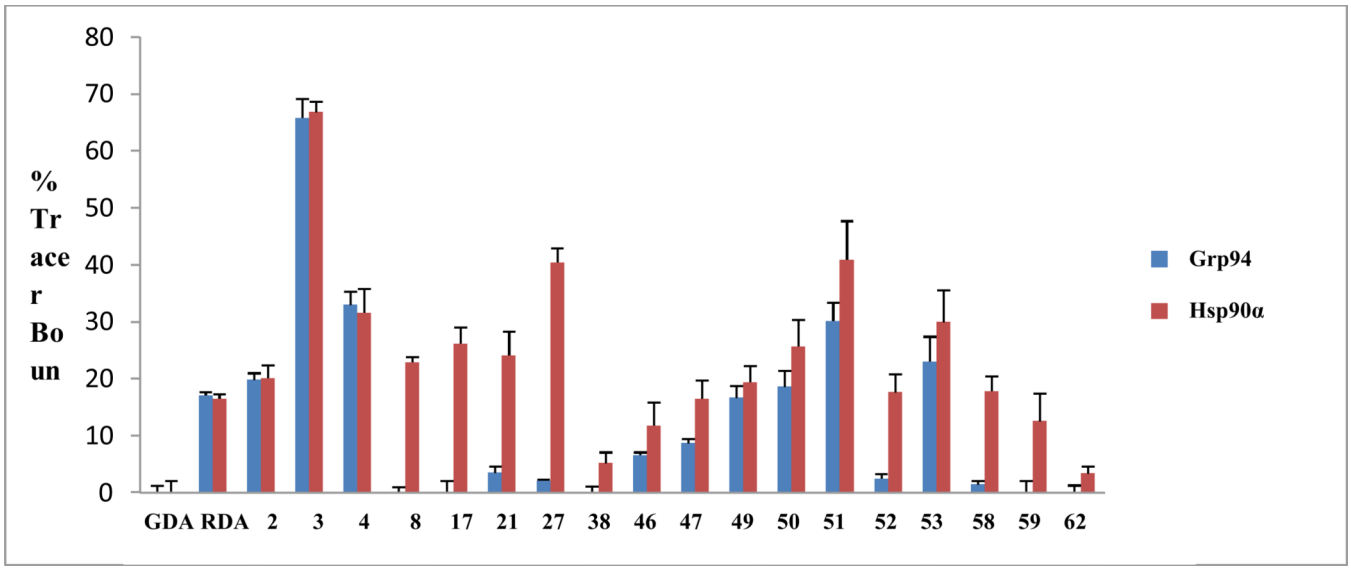

Figure 8.

Inhibition of Grp94 and Hsp90a at 25 μM Illustrating Grp94-Selectivitya–e.

[a] Compounds (25 μM) were incubated with cGrp94 or Hsp90a and FITC-GDA (tracer) for 24 h before fluorescence polarization values were determined. [b] DMSO (1%) served as a negative control (vehicle), and GDA (50 nM) served as the positive control. [c] All compounds tested at 25 μM. [d] All compounds were tested in triplicate

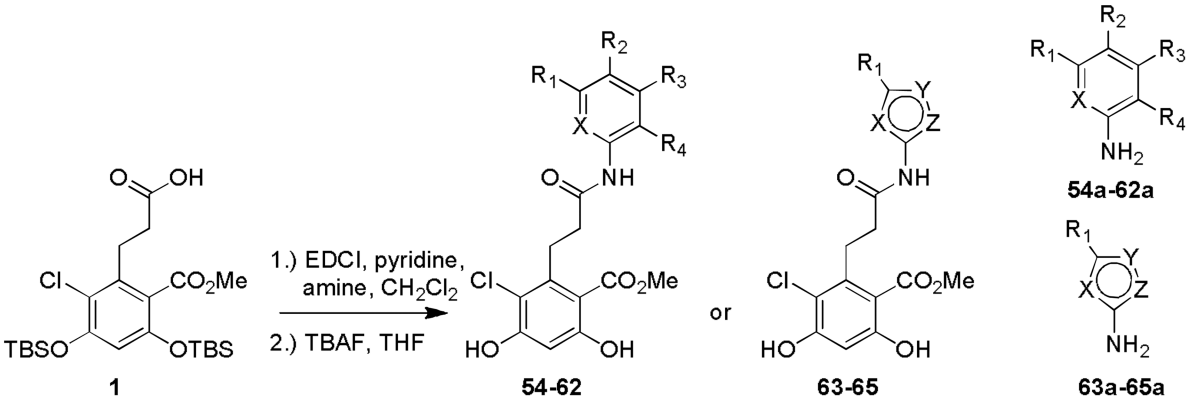

entry	R_1	R_2	R_3	R_4	X	Y	Z	% Tracer Bound
54	H	Br	H	Br	CH			50.7 (±3.3)
55	Cl	H	Cl	H	CH			15.6 (±0.4)
56	Cl	Br	H	H	CH			71.4 (±13.2)
57	H	H	Cl	Br	CH			24.9 (±1.0)
58	Cl	H	H	H	N			1.4 (±0.1)
59	H	Br	H	H	N			0.1 (±0.1)
60	H	H	Cl	H	N			7.7 (±0.3)
61	H	H	H	Cl	N			9.8 (±0.4)
62	H	H	H	Br	N			0.2 (±0.1)
63	Cl				S	CH	N	22.4 (±1.6)
64	Br				S	CH	N	27.7 (±1.8)
65	Br				S	N	N	5.1 (±0.3)

Figure 9.

Combinations of Key Features and their Grp94 Inhibitiona–d

[a] Compounds **54–65** (25 μM) were incubated with cGrp94 and FITC-GDA (tracer) for 24 h before fluorescence polarization values were determined. [b] DMSO (1%) served as a negative control (vehicle), and GDA (50 nM) served as the positive control. ND=not determined. [c] All compounds tested at 25 μM. [d] All compounds were tested in triplicate.

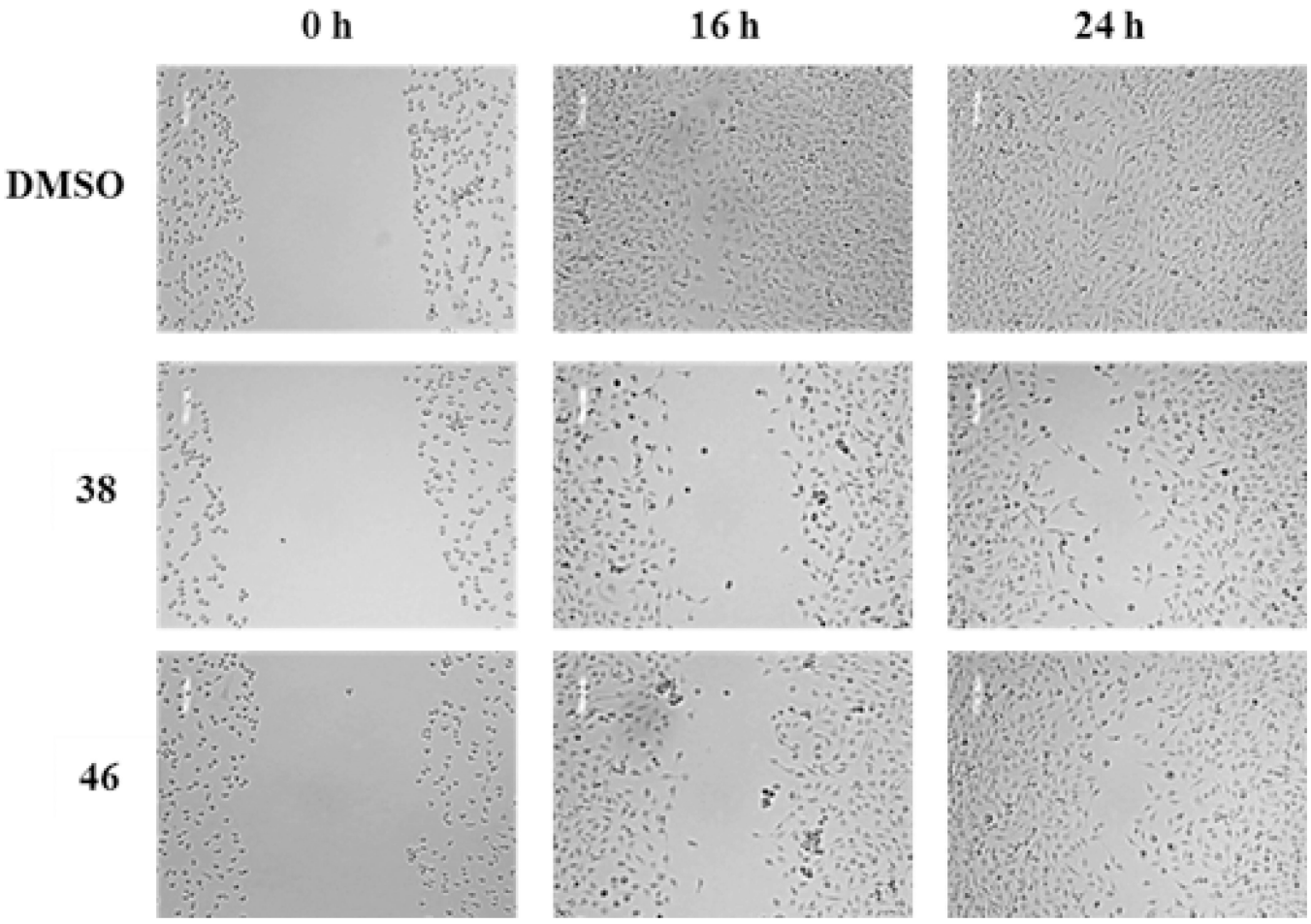

Figure 10.

[a,b] Inhibition of MDA-MB-231 Cell Migration by Compounds **38** and **46**a–b

[a] MDA-MB-231 cells were incubated for 24 h prior to compound addition. [b] Cells were incubated for 16 h and 24 h at 37°C with the respective conjugate indicated above (2.5 μM).

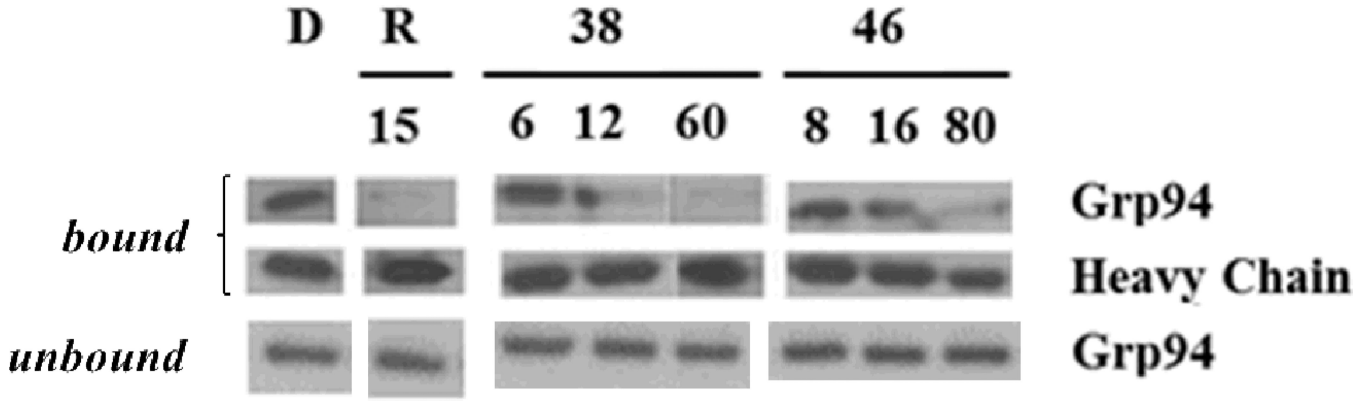

Figure 11.

Effect of compounds **38** and **46** on Grp94 conformation. MDA-MB-231 cells were treated with the indicated concentrations of **38** and **46** (concentrations listed are μM) or radicicol (**R** 15 μM) overnight, and cell lysates were immunoprecipitated with the conformational-specific antibody 9G10 and subsequently were immunoblotted for Grp94. Lower panel, immunoblot of whole cell lysates with 9G10.

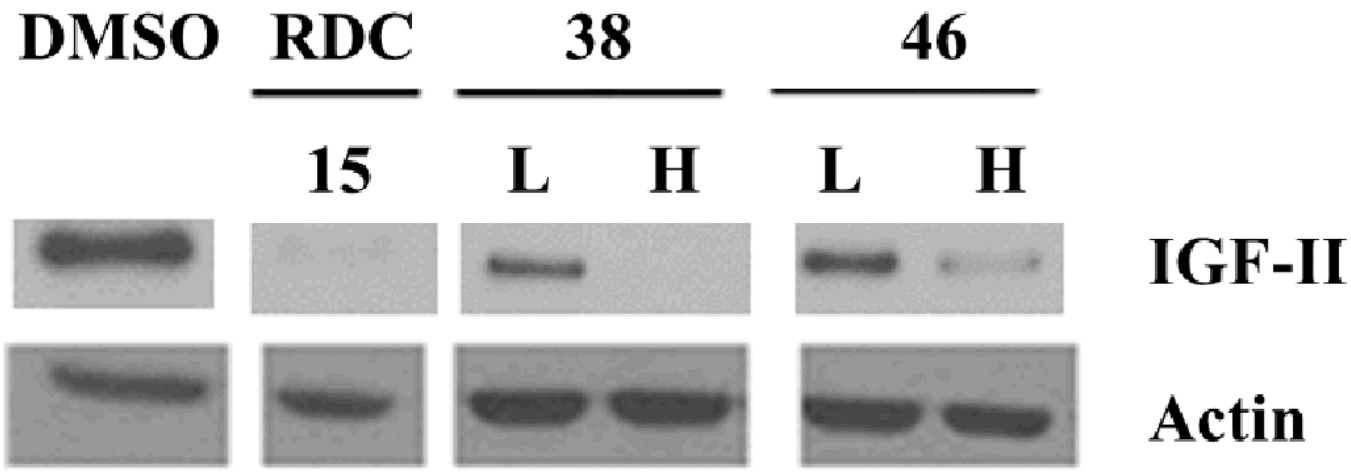

Figure 12.

Western blot analysis of IGF-II secretion into MDA-MB-231 breast cancer cell media upon treatment with amides **38** and **46**. H (high) represents a concentration equal to 10 μM. L (low) represents a concentration equal to 1 μM. Radicicol (RDC, 15 μM) and dimethylsulfoxide (DMSO, 100%) were employed as positive and negative controls, respectively.

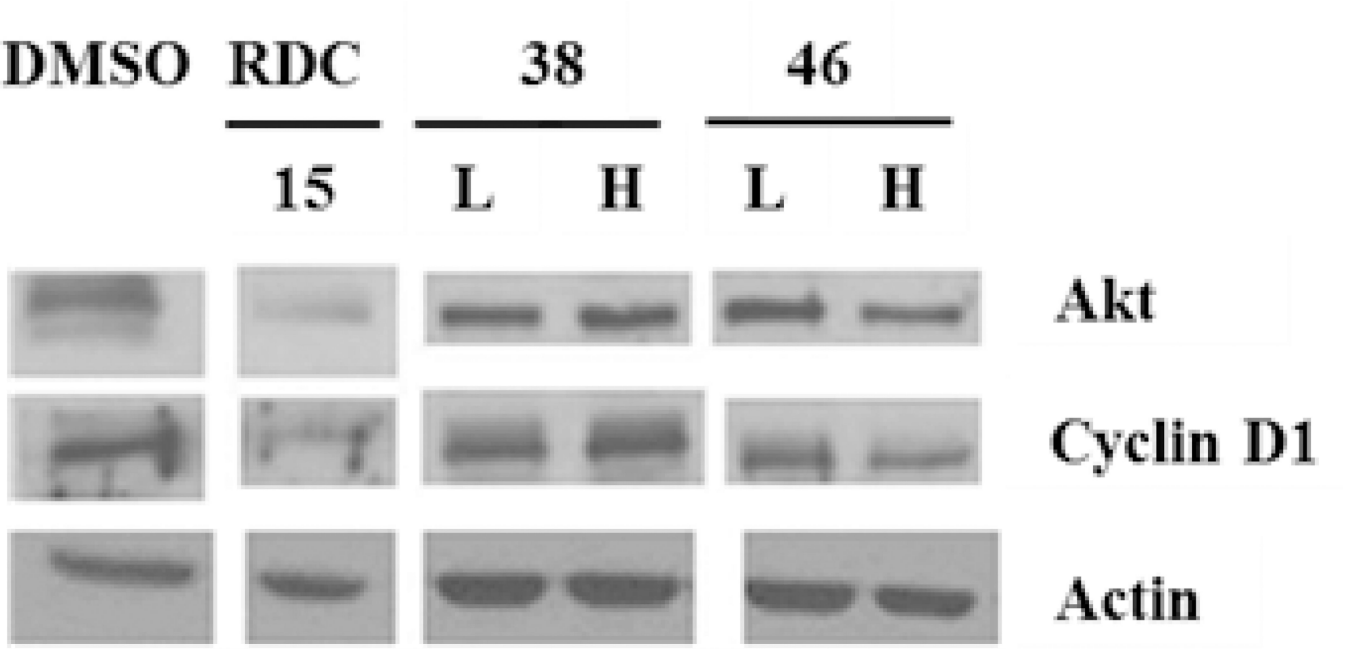

Figure 13.

Western blot analyses of Hsp90-dependent client proteins from MDA-MB-231 breast cancer cell lysate upon treatment with amides **38** and **46**. H (high) represents a concentration equal to 5-fold the anti-proliferative IC_{50} value. L (low) represents a concentration equal to 0.5-fold the anti-proliferative IC_{50} value. Radicicol (RDC, 15 μM) and dimethylsulfoxide (DMSO, 100%) were employed as positive and negative controls, respectively.

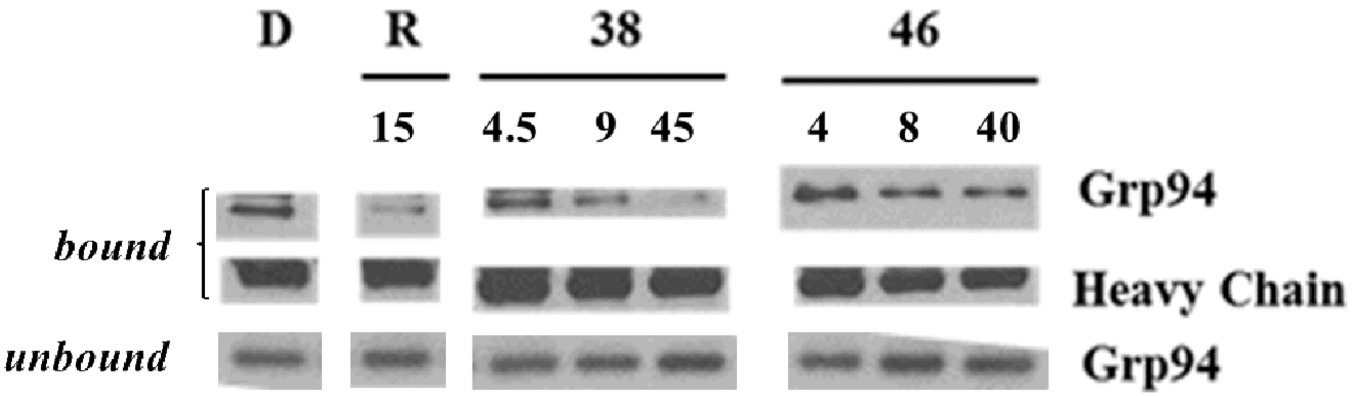

Figure 14.

Effect of compounds **38** and **46** on Grp94 conformation. RPMI 8226 cells were treated with the indicated concentrations of **38** and **46** (concentrations listed are μM) or radicicol (**R** 15 μM) overnight, and cell lysates were immunoprecipitated with the conformational-specific antibody 9G10 and subsequently were immunoblotted for Grp94. Lower panel, immunoblot of whole cell lysates with 9G10.

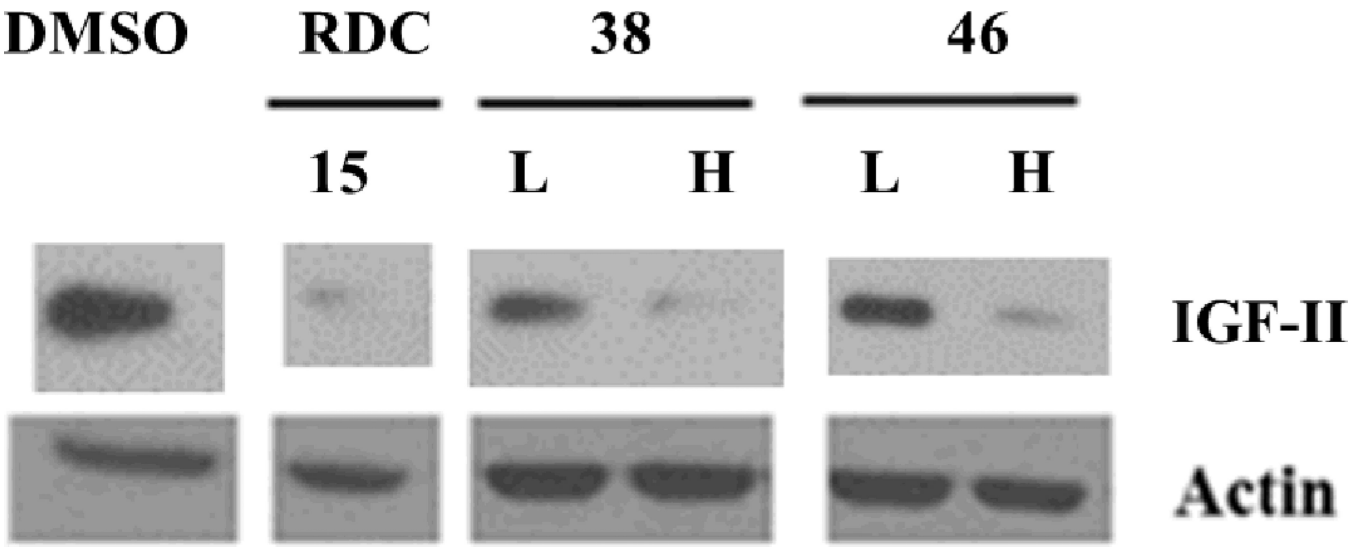

Figure 15.

Western blot analysis of IGF-II secretion into RPMI 8226 cell media upon treatment with amides **38** and **46**. H (high) represents a concentration equal to 2-fold the anti-proliferative IC_{50} value. L (low) represents a concentration equal to 0.25-fold the anti-proliferative IC_{50} value. Radicicol (RDC, 15 μM) and dimethylsulfoxide (DMSO, 100%) were employed as positive and negative controls, respectively.

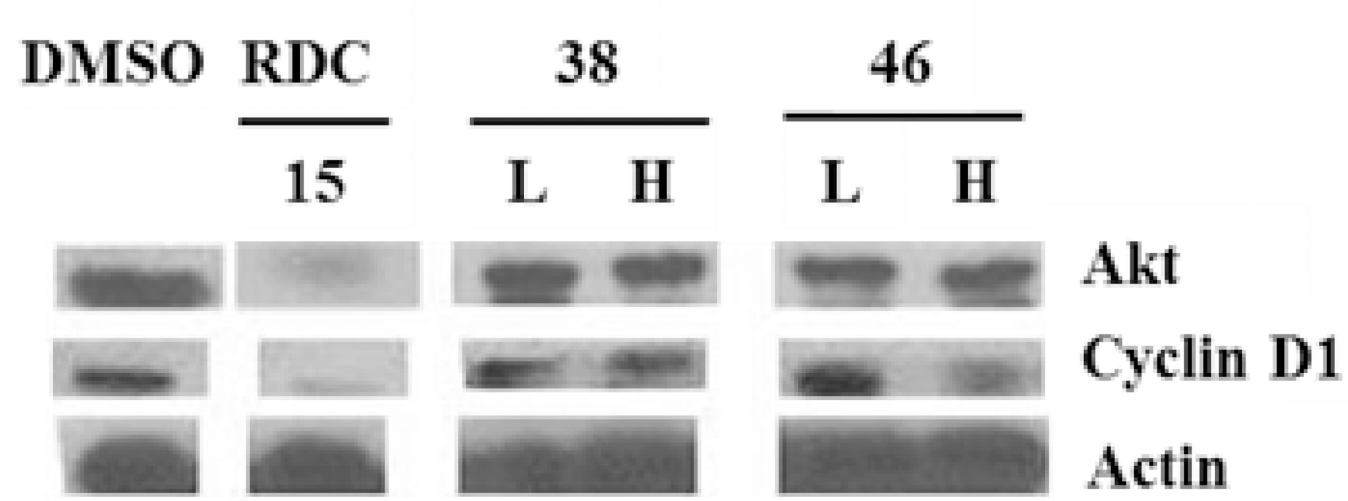

Figure 16.

Western blot analyses of Hsp90-dependent client proteins from RPMI 8226 multiple myeloma cell lysate upon treatment with amides **38** and **46**. H (high) represents a concentration equal to 5-fold the anti-proliferative IC_{50} value. L (low) represents a concentration equal to 0.5-fold the anti-proliferative IC_{50} value. Radicicol (RDC, 15 μM) and dimethylsulfoxide (DMSO, 100%) were employed as positive and negative controls, respectively.

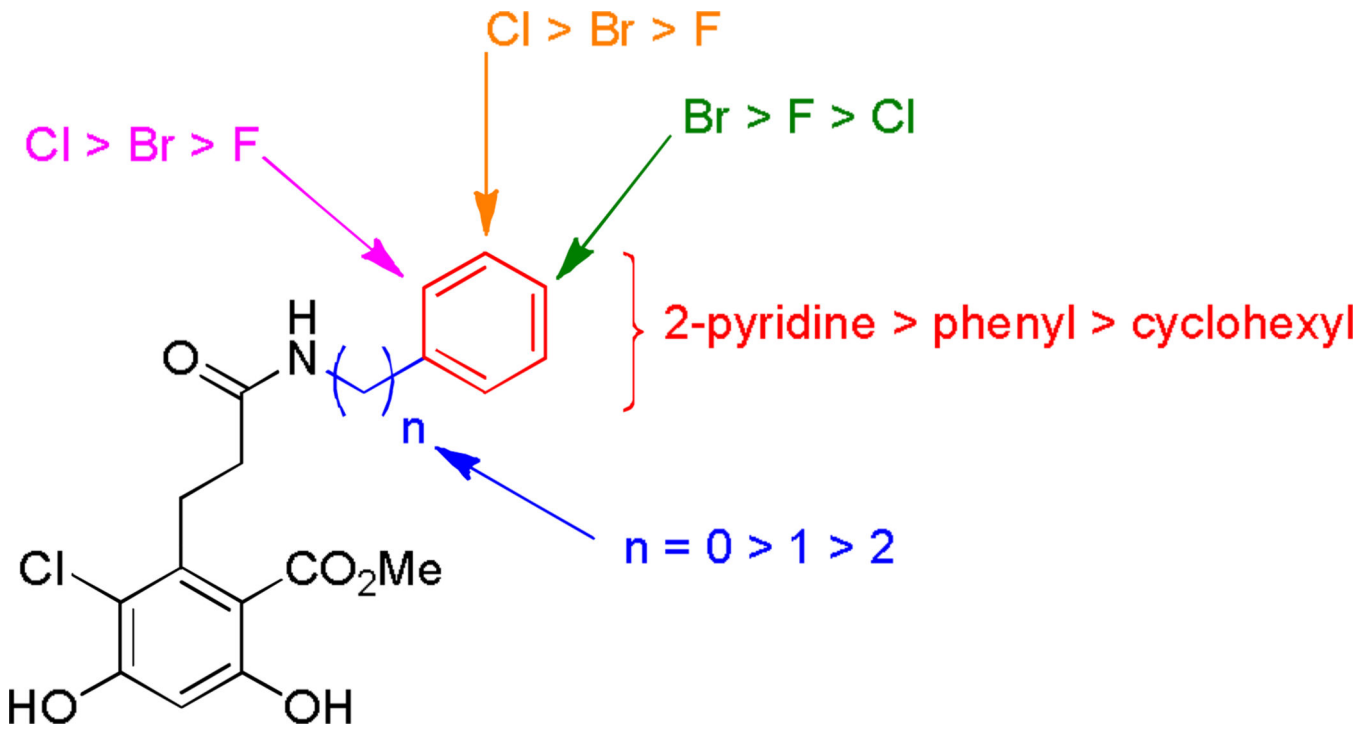

Figure 17.
Summary of SAR for Grp94 Binding of RDA Based Derivatives.

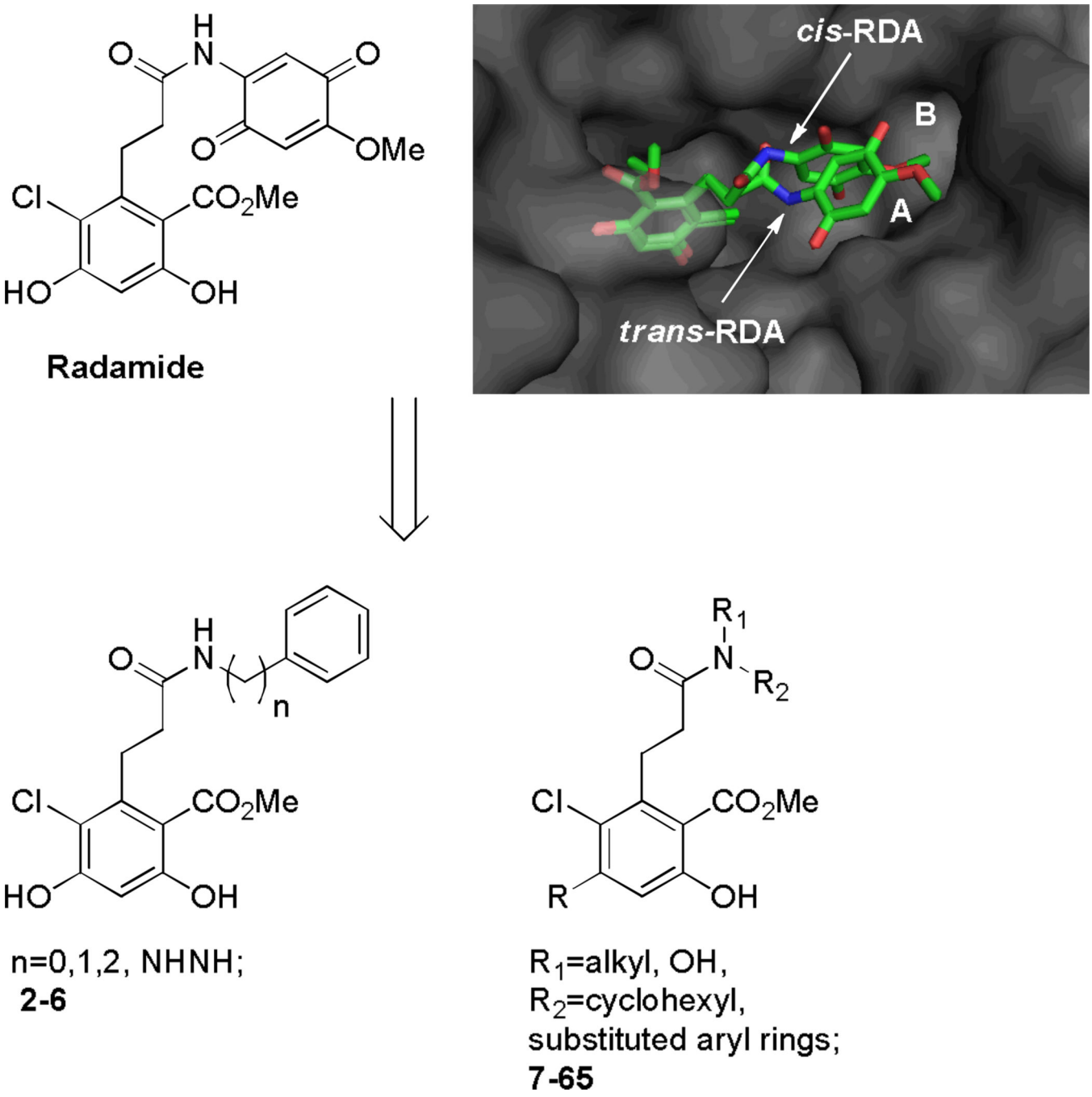

Scheme 1.
Development of RDA-Based Grp94 Inhibitors

Table 1

K_d's of **8, 17, 27, 38**, and **46** for Grp94.[a–d]

entry	K_d (μM)	
8	1.85 (±0.22)	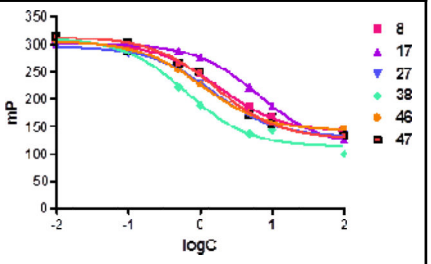
17	6.42 (±0.92)	
27	1.50 (±0.18)	
38	0.82 (±0.09)	
46	1.08 (±0.13)	
47	1.54 (±0.26)	

[a] Compounds **8, 17, 27, 38, 46** and **47** were incubated with cGrp94 and FITC-GDA (tracer) for 24 h before fluorescence polarization values were determined.

[b] DMSO (1%) served as a negative control (vehicle), and GDA (50 nM) served as the positive control.

[c] All compounds were tested in triplicate.

[d] Millipolarization (mP) units were used to determine % tracer bound.

Table 2

[a–c] Anti-proliferative Evaluation of **38** and **46** in RPMI 8226 Cells

entry	IC_{50} (μM)
38	9.12 (±0.4)
46	7.83 (±2.2)

[a] RPMI 8226 cells were incubated for 24 h prior to drug addition.

[b] Cells were incubated for 72 h at 37°C in 5% CO_2 with the respective conjugate.

[c] All experiments were performed in triplicate.